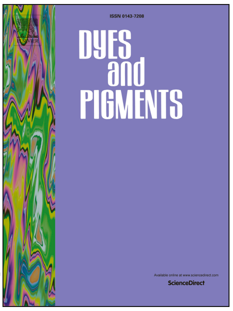

Triketonate difluoroboron complexes. Substitution-dependent liquid crystal and photophysical properties

Ignacio Sánchez, Adrián Fernández-Lodeiro, Elisabete Oliveira, José Antonio Campo, M. Rosario Torres, Mercedes Cano, Carlos Lodeiro

PII: S0143-7208(15)00412-X
DOI: 10.1016/j.dyepig.2015.10.029
Reference: DYPI 4976

To appear in: *Dyes and Pigments*

Received Date: 18 August 2015
Revised Date: 21 October 2015
Accepted Date: 25 October 2015

Please cite this article as: Sánchez I, Fernández-Lodeiro A, Oliveira E, Campo JA, Rosario Torres M, Cano M, Lodeiro C, Triketonate difluoroboron complexes. Substitution-dependent liquid crystal and photophysical properties, *Dyes and Pigments* (2015), doi: 10.1016/j.dyepig.2015.10.029.

Revised version

Triketonate difluoroboron complexes. Substitution-dependent liquid crystal and photophysical properties

Ignacio Sánchez,[a] Adrián Fernández-Lodeiro,[b,c] Elisabete Oliveira,[b,c] José Antonio Campo,[a] M. Rosario Torres,[d] Mercedes Cano,*[a] and Carlos Lodeiro*[b,c]

[a]Department of Inorganic Chemistry I, Faculty of Chemistry, Universidad Complutense de Madrid, 28040 Madrid, Spain. E-mail: mmcano@ucm.es; Fax: +34 91 3944352; Tel: +34 91 3944340.
[b]BIOSCOPE Group, UCIBIO-REQUIMTE, Chemistry Department, Faculty of Science and Technology, University NOVA of Lisbon, Caparica, 2829-516, Portugal. E-mail: cle@fct.unl.pt; Fax: +351 2129 48550; Tel: +351 2129 11402.
[c]PROTEOMASS Scientific Society, Rua dos Inventores, Madam Parque, Caparica Campus, Portugal.
[d]X-Ray Diffraction Laboratory, Faculty of Chemistry, Universidad Complutense de Madrid, 28040 Madrid, Spain.

Abstract

Novel alkoxyphenyl-substituted β,δ-triketonate difluoroboron complexes have been efficiently synthesised and thoroughly characterised. Significant features such as liquid crystal behaviour and solid and solution fluorescence are observed in all cases. The mesomorphism was determined by the presence of one, two or three alkyl chains in each substituent aromatic group of the triketonate ligand. So, smectic C mesophases were found for compounds carrying two lateral chains, each of them located at one of each phenyl substituent, while the presence of four or six chains at the whole molecule gave rise to smectic A or discotic lamellar and hexagonal columnar mesophases, respectively. Fluorescence in the solid state and in solution is again proved to be dependent on the ligand substitution as well as to be maintained in the mesophase. These multifunctional materials also present luminescent sensor activity towards Hg^{2+} and Cu^{2+}.

Keywords: Difluoro(triketonate)boron compounds; liquid crystals; luminescence; bifunctional materials; molecular design

1. Introduction

High-efficiency fluorophores as are the conventional difluoroboron dipyrromethenes (BODIPYs) have been proposed to be used in the field of materials and biological optical imaging [1-3]. However, this kind of compound presents self-quenching related with their small Stokes shifts, so preventing them to be applied as electroluminescent materials in organic light-emitting diodes (OLEDs) [4]. By contrast, the highly emissive β-diketonate-difluoroboron complexes [5-9] have received considerable attention as a potential alternative to emitters in OLED devices [6-9].

In this context, in previous work we have established that the coordination of 1,3-unsymmetrically long-chained alkyloxyphenyl-substituted β-diketonates to the BF_2 fragment give rise to liquid crystal materials which exhibit bent-core mesophases in the range of 120-145 ºC, in addition to an intense fluorescence in the green region [7,8]. However, in designing luminescent liquid crystal materials for technological applications, the supramolecular order of columnar liquid crystals into 2D lattices [10] increases their suitability to these purposes [11]. So, when luminescent columnar liquid crystals are used in the fabrication of OLEDs they can behave as the emissive layer [12]. On this basis we were able to achieve luminescent boron derivatives exhibiting hexagonal columnar mesophases by a strategical control of the ligand established by the employment of polycatenar unsymmetrical β-diketones [9].

Following these results on β-diketonate-difluoroboron complexes as luminescent columnar liquid crystal materials [6-9], we are now involved in extending the study to new boron derivatives by using mono and polycatenar alkyloxyphenyl- substituted β,δ-triketonate ligands towards the BF_2 group. This type of polyketonate ligands have been reported to be useful in achieving complexes with strong intermolecular associations and molecular superstructures as well as to attain homo and heteronuclear bimetallic assemblies, thus leading to multifunctional mesogenic materials with potential magneto and electro-optical applications [13,14].

Currently, our main objective is centred on using β,δ-triketone ligands in which effects like the presence of a largest molecular core, the increasing of the molecular polarisation and the expansion of the π conjugation will be determining factors in order to achieve mesomorphic complexes with improved liquid crystalline properties. In addition, polycatenar systems, which would potentially decrease the phase transition temperatures, have also been strategically used. On the other hand, luminescent liquid crystals having entities able to react to external stimuli are interesting for sensor applications [15,16]. In this context, the BF_2-β,δ-triketonate complexes offer new opportunities as chemosensors towards external metal centres by considering the presence of an uncoordinated oxygen atom as a potential coordinative site. Thus, evaluating the changes on the photophysical properties could be exploited for signalling purposes [17].

In this work, four families of complexes (**Ia**-**Id**) have been prepared. They have been classified according to the number and position of the alkyl chains in the alkyloxyphenyl groups at the 1- and 5-position of the 1,3,5-pentanotrione core (Table 1). For comparative purposes, all the free ligands (**IIa**-**IId**) (Table 1), some of which had already been previously described [13,18], are also included along the study.

2. Experimental Section

2.1. Materials and physical measurements

All commercial reagents were used as supplied. Hydroxybenzoates, *n*-alkyl bromides, tetrafluoroboric acid diethyl etherate, sodium hydride, quinine sulphate, acridine yellow, and the metal salts, $NaBF_4 \cdot xH_2O$, $Ca(OOCCF_3)_2 \cdot xH_2O$, $Zn(BF_4)_2 \cdot xH_2O$, $Pb(BF_4)_2 \cdot xH_2O$, $Cd(OOCCF_3)_2 \cdot xH_2O$, $Ni(NO_3)_2 \cdot xH_2O$, $Co(NO_3)_2 \cdot xH_2O$, $Cu(BF_4)_2 \cdot xH_2O$, $Hg(NO_3)_2 \cdot xH_2O$, $Al(NO_3)_3 \cdot xH_2O$ and $Cr(NO_3)_3 \cdot xH_2O$ were purchased from Stream Chemicals, Sigma-Aldrich or Solchemar.

Elemental analyses for carbon and hydrogen were carried out by the Microanalytical Service of Complutense University (validated range: %C 0.50-94.7, %H 0.50-7.6 and %N 0.50-23.0). IR spectra were recorded on a FTIR Thermo Nicolet 200 spectrophotometer with samples as KBr pellets in the 4000-400 cm^{-1} region: vs (very strong), s (strong), m (medium), w (weak), sh (shoulder). Solution ^1H-, ^{13}C- and ^{19}F-NMR spectra were performed at room temperature on a Bruker DPX-300 spectrophotometer (NMR Service of Complutense University) from solutions in $CDCl_3$. Chemical shifts δ are listed relative to Me_4Si using the signal of the deuterated solvent as reference (7.26 and 77.0 ppm for ^1H and ^{13}C, respectively), and to trifluorotoluene for ^{19}F. Coupling constants *J* are in hertz. Multiplicities are indicated as s (singlet), d (doublet), t (triplet), dd (doublet of doublets), m (multiplet). The ^1H chemical shifts and the ^{13}C and ^{19}F ones are accurate to ±0.01 and ±0.1 ppm, respectively, and coupling constants to ±0.3 Hz. Solid state ^{13}C-NMR spectra of compound **24** have been obtained on a Bruker WB 400 spectrometer (Faculty of

Sciences of the National University of Distance Education) at 300 K using a 4 mm DVT probe head. Samples were carefully packed in a 4 mm diameter cylindrical zirconia rotor with Kel-F end-caps. The mass spectrum of compound **42** was registered on a Bruker Ultraflex MALDI/TOF-TOF spectrometer using dichloromethane as the solvent and dithranol as the matrix.

Phase studies were carried out by optical microscopy using an Olympus BX50 microscope equipped with a Linkam THMS 600 heating stage. The phase transition temperatures were determined from the DSC thermograms by using a Perkin Elmer Pyris 1 differential scanning calorimeter with the sample (1 – 4 mg) sealed hermetically in aluminium pans and a heating or cooling rate of 5 – 10 Kmin^{-1}. X-ray diffractograms at variable temperature were recorded on a Panalytical X'Pert PRO MPD diffractometer in a θ-θ configuration equipped with an Anton Paar HTK1200 heating stage (X-Ray Diffraction Service of Complutense University).

UV-Vis absorption spectra were recorded with a Jasco V-650 spectrophotometer equipped with a Julabo thermostat and the fluorescence emission by a Horiba JY Scientific Fluoromax-4 spectrofluorimeter. The linearity of the fluorescence emission *vs*. concentration was checked in the concentration range used (10^{-5} – 10^{-6} M). A correction for the absorbed light was performed in the case of absorbance (A) higher than 0.2 at the excitation wavelength. The photophysical characterisations were performed using stock solutions of the compounds (*ca*. 10^{-3} M), prepared by dissolving the appropriate amount of the compounds **3**, **5**, **10**, **11**, **15**, **19**, **20**, **24**, **26**, **31**, **32**, **36**, **40** and **41** in dichloromethane in a 10 mL volumetric flask. The stock solutions were then diluted until 10^{-5} – 10^{-6} M. Titrations of **3**, **10**, **11**, **24**, **31** and **32** were carried out by the addition of microliter amounts of standard solutions of the metal ions, Na^+, Ca^{2+}, Zn^{2+}, Cd^{2+}, Cu^{2+}, Hg^{2+}, Al^{3+} and Cr^{3+}, in dry acetonitrile. All measurements were performed at 295 K. Luminescence quantum yields were measured using solution of quinine sulphate in sulphuric acid (0.1 M) [Φ_F = 0.54] for ligands and acridine yellow in ethanol [Φ_F = 0.47] for complexes, as a standard [19]. The values were corrected for different refraction indexes of solvents. Fluorescence spectra of solid samples were recorded using a fibre optic system connected to the Horiba J-Y Fluoromax-4 spectrofluorimeter exciting at appropriate λ (nm) of the solid compounds.

2.2. Synthetic procedures

Ethyl 4-alkyloxybenzoates, ethyl 3,4-dialkyloxybenzoates, methyl 3,5-dialkyloxybenzoates and methyl 3,4,5-trialkyloxybenzoates were prepared by a Williamson alkylation of the corresponding commercially available hidroxybenzoate derivatives [13,20].

2.2.1. Ligands II (21-41)

β,δ-triketones were synthesised by adapting literature methods and fully characterised according to the previous results when corresponding [13,18]. All compounds were characterised by IR and ^{1}H-NMR spectroscopies and elemental analyses. In addition, compound **24** was also characterised by ^{13}C-NMR as a representative example. A procedure for the synthesis and characterisation of a selected compound is given as follows, and the complete characterisation of all the derivatives is deposited in the ESI†.

2.2.1.1. 1,5-Bis-(4’-octyloxyphenyl)-pentane-1,3,5-trione (24).

To a solution of acetone (0.52 g, 9 mmol) and sodium hydride (60 % mineral oil suspension, 2.16 g, 54 mmol) in 1,2-dimethoxyethane (100 mL), ethyl 4-octyloxybenzoate (5.00 g, 18 mmol) was added under N_2 at room temperature. The mixture was then refluxed for 24 h, and the resulting dark brown suspension was cooled to room temperature and poured into ice (*ca*. 200 mL) where the excess NaH was quenched. A small amount of concentrated HCl was added to neutralise the triketone. The product was extracted with chloroform (3 × 50 mL), washed with distilled water (3 × 50 mL) and dried with anhydrous $MgSO_4$. The solvent was removed and the solid residue was recrystallised from tetrahydrofurane/methanol to give 6.75 g of a yellow powder (72 % yield).

Due to the presence of tautomers, ^{1}H- and ^{13}C-NMR signals are listed below and a full assignation is shown in Figs. S1 and S3†.

Mp 103 ºC. Elemental analysis: Found: C, 75.2; H, 8.5%. $C_{33}H_{46}O_5\cdot 0.25H_2O$ requires C, 75.2; H, 8.9%. ν_{max}/cm^{-1}: 3084w ν(O-H), 2932s, 2871s ν(C-H), 1688w ν(C=O)$_{keto}$, 1604s ν(C=C)$_{Ar}$, 1593vs ν(C=O)$_{enol}$, 1567m ν(C=C)$_{enol}$. δ_H (300 MHz; $CDCl_3$; Me_4Si)/ppm: 0.88 (6H, t, ^{3}J 6.6, CH_3), 1.29-1.44 (20H, m, CH_2), 1.80 (4H, m, ^{3}J 6.6, CH_2), 4.02 (4H, t, ^{3}J 6.6, OCH_2), 4.26 (s, $COCH_2CO$), 5.91 (s) and 6.23 (s) (CCHCO), 6.90 (d, ^{3}J 8.9) and 6.92 (d, ^{3}J 8.9) (4H, H_m), 7.80

(d, ${}^3J$ 8.9), 7.82 (d, ${}^3J$ 8.9), 7.92 (d, ${}^3J$ 8.9) and 8.02 (d, ${}^3J$ 8.9) (4H, H_o), 14.87 (s) and 16.08 (s) (OH). δ_C (75.48 MHz; $CDCl_3$; Me_4Si)/ppm: 14.5 (CH_3), 23.1, 26.4, 29.4, 29.5, 29.7, 32.2 (CH_2), 50.8 (C-2), 68.7 (OCH_2), 95.8, 96.4 (C-4), 114.5, 114,8 (C_m), 126.3, 126.6 (C_i), 129.6, 131.7 (C_o), 162.5, 163.4 (C_p), 164.1 (C-5), 173.7 (C-1, C-5), 183.0 (C-5), 189.8, 192.9 (C-3), 193.6 (C-1). δ_C (100.73 MHz; solid; Me_4Si)/ppm: 14.5 (CH_3), 23.7, 27.0, 29.5, 31.2, 31.7, 33.8 (CH_2), 68.3 (OCH_2), 94.9, 95.3 (C-4), 95.0, 97.6 (C-2) 110.6, 112.6 (C_m), 116.2, 118.6 (C_i), 126.6, 129.0 (C_o), 160.5, 161.7 (C_p), 162.7 (C-5), 167.8 (C-3), 173.1 (C-1, C-5), 192.8, (C-1), 193.6 (C-3).

2.2.2. Boron derivatives I (1-20)

The boron derivatives were prepared by adapting a procedure previously reported by us.[9] All compounds were characterised by IR and ^{1}H- and ^{19}F-NMR spectroscopies and elemental analyses. Compound **3** was also characterised by ^{13}C-NMR as a representative example. A general procedure for the synthesis and characterisation of a selected compound is given as follows, and the complete characterisation of all the complexes is deposited in the ESI†.

2.2.2.1. Difluoride(1,5-bis-(4’octyloxyphenyl)-pentano-1,3-dionate-5-one)boron (3)

To a solution of 1,5-bis-(4’-octyloxyphenyl)-pentane-1,3,5-trione (0.523 g, 1 mmol; **24**) in dichloromethane (50 mL), sodium hydride (60 % mineral suspension, 0.042 g, 1.05 mmol) was added. The solution was left to stir for 30 minutes and then tetrafluoroboric acid diethyl ether complex (0.2 mL) were added. After 48 hours of stirring at room temperature, the suspension formed was filtered through a Celite pad and the clear dark green solution was concentrated to obtain a viscous residue, which was purified by silica chromatography using ethyl acetate as the eluent. The solvent was evaporated and the oily product was recrystallised from hexane/methanol to give the title compound as an orange powder (0.37 g, 65 % yield).

Due to the presence of tautomers, ^{1}H-, ^{19}F- and ^{13}C-NMR signals are listed below and a full assignation is shown in Figs. S2 and S4†.

Mp 128 ºC. Elemental analysis: Found: C, 69.6; H, 7.8%. $C_{33}H_{45}BF_2O_5$ requires C, 69.5; H, 7.9%. ν_{max}/cm^{-1}: 2923m, 2853m ν(C-H), 1608s $\nu(C{=}C)_{Ar}$, 1595sh, 1543vs ν(C=O), 1506vs $\nu(C{=}C)_{enol}$, 1383m ν(B-O), 1040s ν(B-F). δ_H (300 MHz; $CDCl_3$; Me_4Si)/ppm: 0.89 (6H, t, ${}^3J$ 6.6, CH_3), 1.29-1.46 (20H, m, CH_2), 1.81 (4H, m, ${}^3J$ 6.6, CH_2), 4.01-4.08 (4H, m, ${}^3J$ 6.6, OCH_2), 4.15

(s, $COCH_2CO$), 5.92 (s), 6.25 (s) and 6.64 (s) (CCHCO), 6.91 (d, ^3J 8.9) and 6.96 (d, ^3J 8.9) (4H, H_m), 7.83 (d, ^3J 8.9), 7.97 (d, ^3J 8.9) and 8.04 (d, ^3J 8.9) (4H, H_o), 11.40 (s, OH). δ_F (282.40 MHz; $CDCl_3$; trifluorotoluene)/ppm: –143.1, –139.7. δ_C (75.48 MHz; $CDCl_3$; Me_4Si)/ppm: 14.1 (CH_3), 22.7, 26.0, 29.1, 29.2, 29.3, 31.8 (CH_2), 52.3 (C-4), 68.5 (OCH_2), 92.6, 94.4 (C-2), 97.1 (C-4), 114.7, 114,8, 115.2 (C_m), 124.1, 124.5, 125.6 (C_i), 129.3, 130.5, 131.3 (C_o), 163.5, 164.2, 166.0 (C_p), 173.7, 179.9 (C-3), 190.7 (C-5), 192.5, 193.2 (C-1), 208.9 (C-5).

2.2.3. Bis(1,5-bis-(4’-octyloxyphenyl)-pentane-1,3,5-trionate)dicopper(II) (42)

The binuclear copper(II) complex containing the ligand **24** was synthesised by a similar procedure to that reported for some of its homologues [13], and characterised by elemental analysis, mass spectrometry and IR spectroscopy.

To a yellow solution of of 1,5-bis-(4’-octyloxyphenyl)-pentane-1,3,5-trione (0.53 g, 1 mmol; **24**) in hot chloroform (20 mL) was added a solution of copper(II) acetate monohydrate (0.22 g, 1.1 mmol) in hot methanol (25 mL). The solution turned green and was refluxed for 3 hours after which it was cooled down to room temperature. The product was filtered off, washed with methanol and recrystallised from a 1:1 mixture of tetrahydrofuran and methanol to yield a dark green powder (0.53 g, 90% yield).

Mp 270 ºC. Elemental analysis: Found: C, 67.4; H, 7.3%. $Cu_2C_{66}H_{88}O_{10}$ requires C, 67.8; H, 7.6%. MS 1068 (M^+). ν_{max}/cm^{-1}: 2919vs, 2853vs ν(C-H), 1606s ν(C=C), 1528vs ν(C=O).

2.3. X-Ray data collection and structure refinement

Data collection for compound **21** was carried out at room temperature on a Bruker Smart CCD diffractometer using graphite-monochromated Mo-Kα radiation (λ = 0.71073 Å) operating at 50 kV and 35 mA. The data were collected over a hemisphere of the reciprocal space by combination of three exposure sets, each exposure of 20 s and covered 0.3º in ω. The first 100 frames were recollected at the end of the data collection to monitor crystal decay, and no appreciable decay was observed. A summary of the fundamental crystal and refinement data is given in Table 2.

The structure was solved by direct methods and refined by full-matrix least-square procedures on F^2 [21]. All non-hydrogen atoms were refined anisotropically. All hydrogen atoms were included in calculated positions and refined riding on the respective carbon atoms, with some exceptions. The hydrogen atoms bonded to oxygen atoms (O1 and O3) were located in a Fourier synthesis and refined riding on the respective bonded atoms.

CCDC 1061994 contains the supplementary crystallographic data for this paper. These data can be obtained free of charge from The Cambridge Crystallographic Data Centre via www.ccdc.cam.ac.uk/data_request/cif.

3. Results and discussion

3.1. Synthetic procedures

All the new complexes **I** as well as their free triketone ligands **II** have been synthesised according to procedures summarised in Scheme 1.

The new triketone ligands **II** (**21**, **22**, **29**, **33-37**, **41**; Table 1) have been prepared according to the method reported by Serrette *et al* [13]. The procedure involves a Claisen condensation between one acetone molecule and two equivalents of the corresponding alkyloxybenzoate **III** (Scheme 1) in the presence of an excess of sodium hydride to give intense yellow powders, which crystallise with a variable number of water molecules. The remaining ligands (**23-28, 30-32, 38-40**; Table 1), which had been previously described [13,18], were again prepared by the same procedure indicated in the literature. Because their full characterisation had not been reported it has been now made and the results will be included along with those of the new related species in order to achieve a systematic study.

The precursor alkyloxybenzoates **III** were synthesised through a Williamson alkylation reaction from the corresponding commercially available hydroxybenzoate derivatives and the appropriate *n*-alkyl bromides. These were carried out in the presence of catalytic amounts of potassium iodide and an excess of potassium carbonate as base, in refluxing acetone for 24-96 hours depending on the number of alkyl chains [13,20].

All the BF_2-triketonate complexes have been obtained by a similar procedure to that used for the related BF_2-diketonate derivatives [9]. The procedure involves the reaction of the corresponding triketone ligand with an excess of tetrafluoroboric acid diethyl ether adduct in the presence of sodium hydride at room temperature. The new complexes were purified by silica chromatography using ethyl acetate (**Ia**) or dichloromethane (**Ib**, **Ic**, **Id**) as a eluent. Recrystallisation from hexane/methanol or chloroform/methanol, respectively, yields stable orange solids whose yellow-green solutions in common organic solvents are visually highly luminescent.

All complexes **I** have been characterised by C, H elemental analysis. In all cases, the one to one relationship BF_2 fragment/ligand was found, in agreement to the proposed formulation. Likewise, the IR and NMR results suggest a mononuclear nature of the compounds, as discussed below.

On the other hand, in order to explore the potential sensorial ability of selected complexes and their corresponding ligands, several metal titrations followed by absorption and emission measurements were performed with Hg^{2+} and Cu^{2+} additions. For additional information and comparative purposes, a Cu(II) complex containing **24** as a ligand was also prepared and characterised. It was synthesised according to a similar procedure described for related triketonate complexes [13], and characterised as the binuclear $[Cu_2(O^{R(8)}OO^{R(8)})_2]$ complex (Scheme 2). The analytical data, the mass spectrum, and the absence of IR bands associated to non-coordinated keto groups in the ligand support the binuclear formulation proposed.

3.2. Structural characterisation

3.2.1. Solution studies of triketone ligands $[HO^{R(n)x}OO^{R(n)x}H]$ II (x = 1, n = 1, 4, 6, 8, 10, 12, 14, 16, 18; x = 2, 3, n = 12, 14, 16, 18). Keto-enol equilibrium

The $CDCl_3$ solution ^{1}H-NMR spectra at room temperature of all the β,δ-triketones (**21-41**) exhibit a similar pattern showing well defined signals from the triketone core and the alkyloxyphenyl substituents. According to a tautomeric equilibrium established in these type of polyketone systems [13,14,22,23], three different keto-enol tautomeric forms can be expected (Fig. 1). In fact, the spectra show two characteristic signals at δ 14.72 – 16.24 ppm, two signals at δ 5.91 – 6.23 ppm and one signal at δ *ca*. 4.26 ppm, assigned for –CO*H*, –CC*H*CO and –COCH_2CO–, respectively (Table 3). The pattern of peaks observed corresponds to the presence of three tautomeric keto-enol forms as depicted in Fig 1. Those are established as the undistinguishable monoenol forms exchanged together by a rapid process (**II$_1$**), and two different dienol forms (**II$_2$** and **II$_3$**) that differ on the position of the keto group within the core, thus giving rise to different chemical shifts of the two dienol tautomers. From the intensity ratio it can be established that the dienol forms are present in a percentage of *ca*. 90%, being the monoenol tautomers the minor ones. The lack of a signal at *ca*. 3.90 ppm indicates the complete absence of the triketo form. The splitting of the aromatic peaks into three signals is also remarkable. Complete assignation of the chemical shifts is included in Fig S1†.

On the other hand it is important to note the observed changes in the spectra of compounds after several months of their synthesis, the new spectra indicating the exclusive presence of the **II_3** tautomer in the solution. This fact suggests the greater stability of this form, which was the same obtained by crystallisation from solutions of **21** (see section below).

^{13}C-NMR spectra in $CDCl_3$ solution support the above results. The presence of the monoenol and dienol forms in the freshly prepared compounds is established from the characteristic shifts of the carbonyl signals of the different tautomers as well as by the splitting of the aromatic signals. Again, after several months from the synthesis of the compounds, their spectra indicate the presence of a sole tautomer.

On the other hand, in the solid state, the ^{13}C-NMR spectra exhibited slightly different spectral features. So, only signals from the two dienol forms (**II_2** and **II_3**) are observed initially, thus indicating the absence of the monoenol tautomer (**II_1**). Further NMR investigation several months after preparation shows that the original mixture evolved to the exclusive presence of the tautomer **II_3**, this fact again confirming that this must be the most stable tautomer among all the possible ones.

Table 4 indicates the characteristic signals observed in the ^{13}C-NMR study in $CDCl_3$ solution and in the solid state for a recently prepared sample of compound **24** selected as a representative example. A detail of the chemical shifts is included in Fig S3†.

IR spectra of all compounds were recorded in KBr at room temperature and, in all cases confirm the exclusive presence of dienol forms in the solid state, as indicated by the absorption bands at *ca*. 3100, 1680 and 1570 cm^{-1} from the ν(OH), ν(CO) and ν(CC) vibrations, respectively, of the enol forms. The lack of a band at *ca*. 1720 cm^{-1} involves the absence of keto groups from the triketo and monoenol tautomers [24]. On the other hand, from the low frequency value of the ν(OH) hydroxyl stretching, strong hydrogen interactions are suggested, as it is expected in dienol forms.

3.2.2. Crystal structure of compound [HO$^{R(1)}$OO$^{R(1)}$H] 21

In order to clarify the tautomeric form in the solid state as well as the structural influence of the triketone ligands for coordinative purposes, we were involved in determining the crystalline structure of these types of compounds. However, all attempts to grow crystals of sufficient quality for single-crystal X-ray analysis were unsuccessful. Then, we synthesised and crystallised a related derivative containing 4-methoxyphenyl substituents at the 1- and 5-position of the pentanotrione core, which, as expected, should crystallise more easily than compounds containing long-chained moieties. Thus, crystals of [$HO^{R(1)}OO^{R(1)}H$] were obtained by slow evaporation of a dilute chloroform solution of the mentioned compound and characterised by single crystal X-ray diffraction.

The molecular structure of [$HO^{R(1)}OO^{R(1)}H$] **21** is depicted in Fig. 2. Table 5 lists selected bond distances and angles. The compound crystallises in the orthorhombic space group $P2_12_12_1$, with four molecules per unit cell.

The molecular structure corresponds to the dienol symmetric form $\mathbf{II_3}$ described in the tautomeric mixture in solution. This tautomer exhibits two enol groups and a keto group at the terminal and central carbon atoms of the ligand backbone, respectively, as deduced from the C – C and C – O distances and the bond angles (Table 5). The presence of non-symmetrical hydrogen bonds between the enol and keto groups with the hydrogen atoms located closer to the oxygen atoms at the terminal positions (Table 6) is also an indicator of this dienol tautomer.

The C – C bond distances in the benzene rings and also in the triketone core are consistent with a delocalised π system. The shape of the molecule is only slightly deviated from planarity. The central backbone is almost planar, with the two planes described by the O3C5C4C3O2 and O2C3C2C1O1 atoms forming a dihedral angle of 5.7(1)º. At the same time, the phenyl groups are deviated from each of these planes 8.2(1) and 3.2(1)º, respectively.

The molecular packing can be described as corrugated layers in which molecules are packed in a *zigzag* disposition. The layers are formed through non-conventional C – O intermolecular interactions between the C12 and O4 atoms of neighbouring molecules, with a distance of 3.45(1) Å (symmetry operation; $-x + ½ + 1$, $-y + 1$, $z + ½$), but no significant interactions are found between layers (Fig. 3).

3.2.3. Difluoroboron complexes [$BF_2(HO^{R(n)x}OO^{R(n)x})$] I (x = 1, n = 4, 6, 8, 10, 12, 14, 16, 18; x = 2, 3, n = 12, 14, 16, 18)

^{1}H, ^{19}F and ^{13}C-NMR spectra of all difluoroboron-β,δ-triketonate complexes **I** (**1**-**20**) have been recorded in $CDCl_3$ solution at room temperature.

The presence of an uncoordinated free oxygen atom not bonded to the BF_2 fragment in the triketonate backbone leads to the two posible keto-enol tautomers, as depicted in Fig. 4. This result was found for **Ia** and **Ic** complexes, as it was deduced by the splitting of the triketonate core and aromatic signals observed in the ^{1}H and ^{13}C-NMR spectra, as well as by the presence of two fluorine signal peaks in the ^{19}F-NMR measurements. By contrast, spectra of **Ib** and **Id** compounds indicate the presence of the keto tautomer exclusively.

For **Ia** and **Ic** compounds, exhibiting the keto-enol equilibrium, three ^{1}H-NMR methyne signals in the range of δ 5.92 – 6.64 ppm, one methylene signal at 4.15 ppm and one hydroxyl signal at 11.40 ppm are consistent with the presence of both enol and keto tautomers (Fig. 4). A strong coordination to the BF_2 fragment is deduced from the shift of the methyne central protons signals of the triketonate core to lower fields related to the free neutral β,δ-triketones. In addition, the large shift to upper fields of the hydroxyl peak suggests that this group should be involved in a strong hydrogen interaction with the neighbouring fluorine atoms in the enol form.

Two fluorine signals in the ^{19}F-NMR spectra related with the two tautomers are observed in a range of -139 to -143 ppm. Each of them is duplicated and consists in two sharp lines with an intensity ratio of 1:4, in agreement to the natural abundance of the two boron isotopes, ^{10}B and ^{11}B.

The ^{13}C-NMR spectra show carbonyl, methyne and methylene carbon signals in their characteristic regions, being low-field shifted with respect to those of the neutral ligands by effect of the coordination.

Table 7 recovers the most characteristic NMR signals of **3** as a representative example. A complete assignation is shown in figures S2 and S4†.

In the keto-enol mixture of **Ia** and **Ic**, the enol tautomer was found in the highest percentage as deduced from the intensity ratio of the ^{1}H-NMR methyne/methylene signals (60:40). By contrast, derivatives of **Ib** and **Id** types showed a single peak due to the keto form, this fact can be related with the enhanced steric effect produced by the presence of two or three adjacent chains in the phenyl substituents. Therefore, as the keto form is less restrained to planarity, the equilibrium should be shifted to this tautomer, allowing a better accommodation of the voluminous groups.

IR spectra of the complexes in the solid state exhibit characteristic bands of enolate groups at *ca*. 1540 and 1500 cm^{-1} associated to the ν(CO) and ν(CC) stretching absorptions. These bands are noticeably bathochromically shifted with respect to those of the neutral ligand, so indicating the strong coordinative interaction with the BF_2 fragment, in agreement with the ^{1}H-NMR results. The carbonyl band at *ca*. 1595 cm^{-1} from the neutral enol group along with the absence of a keto band at *ca*. 1720 cm^{-1} indicate that the enol form is the unique tautomer in the solid state for all the boron derivatives. Bands at *ca*. 1380 and 1030 cm^{-1} from the ν(BO) and ν(BF) stretching vibrations complete the main absorptions of the complexes [24].

3.3. Thermal behaviour

Thermal properties of the free triketone compounds **II** as well as those of their corresponding boron complexes **I** were studied by polarised optical microscopy (POM), differential scanning calorimetry (DSC) and X-ray diffraction at variable temperature, the latter technique used only in representative complexes. Tables 8 and 9 list the phase transition temperatures and their corresponding enthalpies established by DSC.

3.3.1. Triketone derivatives [$HO^{R(n)x}OO^{R(n)x}H$] II (x = 1, n = 4, 6, 8, 10, 12, 14, 16, 18; x = 2, 3, n = 12, 14, 16, 18)

None of the new triketone ligands **II** exhibited liquid crystalline behaviour in agreement to the absence of mesomorphism of the related derivatives previously reported [13,18]. However, for the latter the thermal results had not been explicitly mentioned and so, we were interested to compile the melting temperatures of all the ligands used in this work. Phase transition temperatures on heating of compounds **II** are depicted in Table 8.

POM observations show direct melting from the solid to the isotropic liquid at a temperature range depending on the degree of alkyloxy substitution at the aromatic groups. On the other hand, several solid phases are observed prior to the melting.

Variations in the melting temperatures were analysed as depending on the number, position and length of the alkyl chains attached to the phenyl substituents (Fig 5). Polycatenar ligands **IIc-IId** show their melting transition at lower temperatures that those of the monocatenar ligands **IIa**, this fact suggesting a less effective packing in the solid state for the former ones. In addition, the results reveal a quite different behaviour for each family of compounds, suggesting that a slight change in the molecular structure translates in to a large modification of their properties.

For compounds of families **IIa**, with monocatenar aryl groups, and **IIc**, carrying two chains at the *meta* positions of the aryl group, the melting temperatures do not seem to be notably modified by increasing the alkyl chain length, so suggesting that interpenetration between chains is not favoured, as an increase in the melting point by increasing the alkyl length should be expected. By contrast, the opposite behaviour was found for compounds of series **IIb** carriers of adjacent chains at each aromatic substituent group, at difference of the alternating positions they occupy in compounds **IIc**. In this series **IIb** a decrease of the melting temperatures by increasing the alkyl chain length was observed. Therefore, we propose a higher packing efficiency potentially due to lower mobility of the chains, which should be restricted in relation to that of the compounds **IIa** and **IIc**. The decrease of the melting temperatures by increasing the chain length could be explained on the basis of less effective alkyl interpenetration when longer chains are present.

Finally, opposite results were observed for the most substituted compounds **IId** which should exhibit the lowest melting temperatures. However, the melting occurs at higher temperatures by growing the alkyl length, thus indicating that the alkyl chain interdigitation effect is balanced by the increment of the Van der Waals forces. In addition, lower molecular mobility would lead to a more effective packing in the solid, thus leading to higher values of the melting temperatures in comparison to those of family **IIc**.

3.3.2. Difluoroboron triketonate complexes $[BF_2(HO^{R(n)x}OO^{R(n)x})]$ I (x = 1, n = 4, 6, 8, 10, 12, 14, 16, 18; x = 2, 3, n = 12, 14, 16, 18)

All the complexes of families **Ib**, **Ic** and **Id** as well as compounds **7** and **8** from **Ia** exhibit enantiotropic liquid crystal behaviour as revealed by POM observations and DSC thermograms. The thermal properties of all the new adducts are collected in Table 9. In Figs. 6a, 7a, 8a and 9a the stability range of the mesophases is depicted for a better quality of discussion.

It is interesting to remark that each family of compounds exhibit different mesophases, this fact being related to their corresponding molecular geometry. Thus, a smectogenic behaviour has been found for compounds **Ia**, containing monocatenar alkyoxyphenyl-substituted triketonate ligands, and **Ib**, carriers of two adjacent alkyl chains at each aromatic ring of the ligand, while the discotic nature of the derivatives **Ic,** with two separate alkyl chains, and **Id**, with three chains in each aromatic group, leads to discotic lamellar and columnar mesophases, respectively.

For compounds of family **Ia**, only those with long-tailed substituents **7**, **8** (n = 16, 18) exhibited liquid crystal behaviour, while those derivatives with shorter alkyl chains (n < 14) were not mesomorphic, showing crystalline polymorphism and a direct melt to the isotropic liquid (Fig. 6a). Compounds **7** and **8** exhibit enantiotropic SmC mesophases, as deduced from the POM observed characteristic *Schlieren* texture [25] (Fig. 6b). Their DSC thermograms show, on heating, an endothermic peak related to a solid-solid phase transition followed by two overlapped peaks from the solid-mesophase and mesophase-isotropic liquid transitions, in agreement with the POM observations. On cooling, the mesophase was undoubtedly identified by the characteristic *Schlieren* texture, previous to the crystallisation, but in the DSC traces only a wide peak corresponding to both overlapped transitions was observed. The mesophase ranged between 114 – 122 ºC. The melting temperatures were the same for both **7** and **8** derivatives, but **8** exhibits a higher clearing temperature, so indicating a slight expansion of the mesophase range by increasing the alkyl length.

As an interesting feature it can be mentioned that, contrarily to the results reported by us on monocatenar symmetrically alkoxyphenyl-substituted β-diketonate containing difluoroboron complexes, which were not mesomorphic [6], the new long-tail monocatenar aryl-substituted triketonate derivatives behave as liquid crystals. This fact can be explained on the basis of the requirement of an appropriate width-to-length molecular ratio, which seems to be favoured with the longest chains and the most extensive core of the triketones, besides of their increased and extensive conjugation.

Complexes belonging to series **Ib** (**9-12**) also present a smectogenic mesomorphic behaviour. The melting transition was easily detected by POM on heating by the appearance of a phase with intense birefringence and high mobility, which happens in the range of 27 – 65 ºC depending on the alkyl length. The presence of focal-conic domains and oily strikes on the borders of the preparation agrees with its assignation as a SmA mesophase [25] (Fig. 7b). By increasing the temperature, the mesophase solidifies in all cases between 54 and 75 ºC giving rise to the break-up of the mesophase texture as well as a loss of the mobility. After the solidification, a melting to the isotropic liquid occurs. DSC thermograms agree with this behaviour showing an exothermic peak followed up by an endothermic peak related to the melting of the solid phase. On cooling from the isotropic liquid, the mesophases were poorly detected by POM prior to the crystallisation and, according to that, in the DSC thermograms only a peak related to crystallisation could be observed, both facts indicating that the mesophase formation involves a very slow process. As depicted in Fig. 7a, the increase of the alkyl chains length leads to higher values of the phase transition temperatures, being the stability range of about 10 ºC for all complexes with the exception of complex with 12 carbon atoms at the alkyl chains, which, due to its noticeable low value of the melting temperature the mesophase shows a stability range of 27 ºC before the crystallisation.

Concerning compounds of family **Ic**, all of them **13-16** exhibit a similar liquid crystal behaviour. Observation by POM at the typical rate of 10 Kmin^{-1} failed to identify the mesophase structure since only a viscous appearance was observed on heating before the isotropic liquid was formed. However, further experiments using a rate of 1 Kmin^{-1} allowed us to observe the appearance of a birefringent fibrous texture which was maintained until the isotropisation of the sample. On cooling from the isotropic liquid, the compounds were allowed to cool slowly at 1 Kmin^{-1} in steps of 5 ºC and the temperature maintained in each step for 3 hours until appearance of the mesophase, thus allowing us to observe the formation of a stable broken fan-like texture (Fig. 8b) characteristic of discotic lamellar structures (Col$_L$) [26,27]. Finally, after 12 hours at room temperature, crystallisation of the sample was shown.

DSC thermograms made up at 10 Kmin^{-1} only show a wide endothermic peak on heating corresponding to both melting and clearing overlapped transitions. Due to the low phase transition temperatures and the slow cooling rate needed to detect the mesophase on cooling, no further DSC experiences were able to be attempted in order to confirm the behaviour exhibited by POM.

Bar diagram of Fig. 8a shows the stability range of the Col$_L$ mesophase as a function of the alkyl length. It is remarkable that, the mesophases appear at temperatures of 50 – 60 ºC and are maintained until 61 – 77 ºC. As usual, the Van der Waals forces are enhanced by increasing the alkyl length leading to an increment of the melting and clearing temperatures. The stability ranges increase following the same tendency, thus the widest range being found for compound **16** with *n* = 18 carbon atoms at the alkyl chains.

The POM observations of compounds **Id** (**17-20**) indicate enantiotropic mesomorphism. On heating from the solid, a birefringent phase is formed, with the exception of the compound bearing the shortest chains **17** (*n* = 12) that exhibits this phase at room temperature. On cooling from the isotropic phase, a dendritic texture with linear birefringent defects could be observed, subsequently giving rise to a mosaic texture with pseudo-focal conic regions, which is typical of the hexagonal columnar mesophases [26,28,29] (Fig. 9b). DSC thermograms confirm this behaviour, showing the corresponding endothermic peaks on heating as well as the exothermic ones related to the reverse phase transitions. As depicted in the bar diagram (Fig. 9a), both melting and clearing temperatures are increased by growing the alkyl length, as was observed for the analogue **Ia**-**Ic** complexes. Also the stability range tends to decrease, the best results being achieved for the shorter-chain derivative of the family which exhibits the Col_h mesophase at room temperature and with a range of *ca.* 35 ºC.

3.3.3. Comparative results from thermal behaviour of Ia-Id complexes

By comparing the mesomorphism of the different families of boron-complexes, several conclusions can be established.

Firstly, by comparing the results of the new complexes to those previously reported on related β-diketonate complexes [6-9], it has been established that the presence of the larger molecular rigid core, involving an expansion of the π conjugation and the molecular polarisation has been a useful tool to induce mesomorphism in the difluoroboron complexes. Therefore, the efficiency of the β,δ-triketonate ligand core to achieve mesomorphic complexes has been proved.

On the other hand, it should be mentioned that in the β-diketonate systems, the molecular asymmetry related to the length at the chains at both substituents, and/or the presence of a different number of alkyl chains at both phenyl rings was a requirement in order to achieve mesomorphic complexes [7-9]. However, this requirement was not necessary when using β,δ-triketonate ligands towards the BF_2 group, in which liquid crystal behaviour was always achieved, even at room temperature.

We have also been able to modulate the type of mesomorphism by the controlled design of the ligands, the molecular geometry being the main feature that governs the type of mesophase. That is imposed by the number and position of the alkyl chains at the aromatic substituents at the 1- and 5-positions of the triketone core. Thus, compounds bearing one chain or two adjacent chains in each phenyl group display smectogenic behaviour, in agreement to the rod-like molecular shape. By contrast, disk-shaped complexes are achieved when two alternate or three alkyl chains are attached to the aromatic substituents. As a consequence, the complexes exhibit lamellar discotic or hexagonal columnar mesophases, respectively.

It is also of interest to compare the phase transition temperatures of the complexes of the four families in order to establish which of them present the best liquid crystal properties. So, while the monocatenar derivatives **Ia** show the higher melting and clearing temperatures, and the narrower stability ranges of the mesophase, opposite results were found for complexes **Ib**-**Id**. Thus, it seems that the use of polycatenar systems is a determinant factor to achieve lower transition temperatures, thus giving rise to more suitable materials for technological applications.

Among the polycatenar compounds **Ib**-**Id**, it is noticeable that in each family, the melting and clearing temperatures were higher for those with longer flexible chains, determining that the presence of shorter chains appears as a requirement to achieve mesogens at nearly room temperature.

On the other hand, the melting temperatures are in a similar range for compounds **Ib** and **Id**, while those of complexes **Ic** are slightly higher. In addition, since the clearing temperatures are much higher for members of family **Id** and the mesophases of **Ib** suffer crystallisation upon heating, the range of the mesophase is extended about 10 ºC, 15 ºC and 30 ºC for complexes **Ib**, **Ic** and **Id**, respectively. Therefore, it seems that the discotic six alkyl chains peripherally-decorated complexes present the best liquid crystalline properties.

3.3.4. Temperature-dependent powder X-ray diffraction studies

Variable-temperature powder X-ray diffraction experiments were performed on selected mesomorphic compounds from **Ia**-**Id** to confirm the structure of the mesophases observed by POM. The results are summarised in Table 10.

Fig. 10 depicts the diffractogram of compound **7**, selected from **Ia**, at 115 ºC on heating, temperature at which the mesophase have been proved to be present. Two sharp peaks in a 1 : 1/2 ratio indexed as the (001) and (002) reflections are indicative of a lamellar structure. In addition, a broad halo in the medium-angle region at *ca*. 4.5 Å corresponds to the liquid-like order of the molten alkyl chains. This pattern appears in both heating and cooling processes, indicating the enantiotropic behaviour of the compounds. From the above result as well as the observed *Schlieren* texture, a SmC structure was assigned for all the mesophases of **Ia** compounds.

The identification of the smectic mesophase of compounds belonging to family **Ib** has been harder since the mesophase subsequently crystallises upon heating. This feature prevented us obtaining diffractograms free of peaks from a solid phase. In particular, Fig. 11 shows the diffractogram of compound **12** at 68 ºC, temperature where the mesophase could be observed although overlapped with a crystalline phase which starts to be formed. Four sharp peaks with a *d*-spacing ratio of 1 : 1/2 : 1/3 : 1/4 are associated to the (001), (002), (003) and (004) reflections, thus confirming its smectogenic behaviour previously established for this family of derivatives.

The $\mathrm{Col_L}$ mesophase of compounds **Ic** was undoubtedly confirmed from the diffraction patterns of compounds **15** and **16** recorded at temperatures of mesophase existence. In both cases, the diffractograms show, both the heating and cooling, two or three peaks from the (001), (002) and (003) reflections with a *d*-spacing ratio of 1 : 1/2 : 1/3 of a lamellar phase. In addition, a diffuse band indicating the liquid-like order of the molten chains was localised around 4.5 Å.

Finally, the $\mathrm{Col_h}$ nature of the mesophase of compounds **Id** could be extrapolated from the diffraction patterns of compounds **19** and **20** recorded at temperatures at which the liquid crystal state had been reached (Fig. 12). These exhibit a strong fundamental maximum in the low angle region from the (100) reflection, followed up by a set of weak peaks with a *d*-spacing ratio of 1 : 1/√3 : 1/√4 : 1/√7, corresponding to the (110), (200) and (210) reflections of a hexagonal columnar phase. In addition, a broad band from the (001) reflection with a *d*-spacing value of 3.4 Å is consistent with a π-π stacking between mesogenic units of each column. The broad diffuse band at *ca*. 4.5 Å is again related to the fluid order of the alkyl chains in the mesophase.

3.4. Photophysical studies

The photophysical studies of the free ligands **II** and their BF_2 complexes **I** have been carried out in such a way that factors related to the number, position and length of the alkyl chains were analysed to establish their influence on the luminescent properties. Thus, the luminescent behaviour of ligands **24** and **26** (**IIa**), **31** and **32** (**IIb**), **36** (**IIc**), **40** and **41** (**IId**) as well as their counterpart complexes **3** and **5** (**Ia**), **10** and **11** (**Ib**), **15** (**Ic**) and **19** and **20** (**Id**) has been fully studied.

3.4.1. Photophysical characterisation

The absorption, emission and excitation spectra of the β,δ-triketone ligands **II** (**24**, **26**, **31**, **32**, **36**, **40**, **41**) and their complexes **I** (**3**, **5**, **10**, **11**, **15**, **19**, **20**) were measured in dichloromethane solutions (*ca*. 10^{-5} – 10^{-6} M) at 295 K. The emission spectra in the solid state of all compounds were also recorded. The photophysical data obtained are gathered in Table 11.

The β,δ-triketone derivatives **II** show absorption bands centred at *ca*. 391-409 nm, which are characteristic of the electronic π-π* transition of chelating β-ketonate ligands [5-9,30], while the maximum in the difluoro(triketonate)boron complexes **I** is centred at *ca*. 433-474 nm.

Regarding the emission, it was observed that complexation of the free ligands to the BF_2 fragment led to a general red spectral shift, the spectra showing in all cases a broad band with an unresolved vibronic substructure at *ca*. 418-470 nm for **II** and at *ca*. 483-525 nm for **I**.

On the other hand, no significant spectral variations were produced by the increasing of the carbon atoms in the lateral-side chains in complexes **3**, **5** (**Ia**) and **10**, **11** (**Ib**) as well as in the ligands **24**, **26** (**IIa**) and **40**, **41** (**IId**).

Concerning the ligands, the increase of the number of alkyl chains from two to four or six in **24**, **26** (**IIa**), **31**, **32** (**IIb**) and **36** (**IIc**), and **40**, **41** (**IId**), respectively, practically does not affect the ground state of the molecules. By contrast, in the excited state the position of the maximum appears to be dependent on the number of alkyl chains at the aryl substituents, as visible red shifts from 442 nm to *ca*. 450 nm and to *ca*. 470 nm of the emission bands are detected in the above compounds (**24**, **26**; **36**; **40**, **41**). This fact can be due to the strong electron-donating effect of the alkyl groups produced by the increase in the number of alkyloxy chains. The degree of substitution lowers the energy gap and changes the electronic distribution. This aspect had already been observed in our previous difluoroboron alkyloxyphenyl-β-diketonate systems [6-9].

Related to the boron complexes, the increment of the number of alkyl chains from two in **3** and **5** (**Ia**) to four in **15** (**Ic**) again does not produce significant variations while the presence of six chains in **19** and **20** (**Id**) led to a red shift in the absorption and emission bands, this feature being explained on the basis of the higher electron donation towards the BF_2 group.

On the other hand, the position of the alkyl groups in the compounds containing four chains (**31**, **32** (**IIb**), **36** (**IIc**), **10**, **11** (**Ib**), **15** (**Ic**)) is also a factor that modifies the spectral behaviour. Derivatives of **Ib** and **IIb** types, in which both chains at each substituent are adjacent, show absorption bands at higher energy compared to those of **Ic** and **IIc** types with separated chains (Table 11), concluding that the electron donor effect of the alkyl groups is somehow enhanced when the two groups are in *meta* relationship one to each other.

The relative fluorescence quantum yield was calculated using quinine sulphate and acridine yellow as a standard for ligands and complexes, respectively. All the studied ligands **II** show low fluorescence quantum yields (ϕ) at *ca*. 0.003-0.05. However those increased in the boron complexes **I**, the highest values being observed for **3**, **5** (**Ia**; ϕ = 0.34-0.36) and **10**, **11** (**Ib**; ϕ = 0.67-0.71). Surprisingly, the position of the chains seems to be a more influent factor to decrease the quantum yields than the number of alkyl chains attached to the aromatic groups, as it was expected. As the quantum yield is decreased in complexes **Ic** and **Id**, we suggest that the presence of a flexible group at the 5-position of the phenyl ring tends to decrease the fluorescence efficiency of the molecule. This fact can be probably attributed to a higher flexibility in the excited state which would increase the non-radiative decay processes [6].

Regarding the emission in the solid state, a broad band peaked at *ca*. 487-520 nm and at *ca*. 543-600 nm is observed for the β,δ-triketone derivatives **II** and boron complexes **I**, respectively. All emission bands observed in the solid state spectra are bathochromically shifted with respect to the ones measured from the spectra in solution. As a representative example, Fig. 13 depicts the full photophysical characterisation of **3** (**Ia**) as well as that of its precursor β,δ-triketone **24**.

4.2. Sensorial ability towards metal ions

In order to explore the potential sensorial ability of the β,δ-triketone derivatives **II** and that of their boron complexes **I**, several metal titrations followed by absorption and emission measurements were performed in dichloromethane solution with the increasing addition of Na^+, Ca^{2+}, Zn^{2+}, Cd^{2+}, Pb^{2+}, Cu^{2+}, Ni^{2+}, Co^{2+}, Hg^{2+}, Al^{3+} and Cr^{3+} in dry acetonitrile. For that purpose, the metal titrations were carried out with the ligands **24** (**IIa**) and **32** (**IIb**), and their boron complexes **3** (**Ia**) and **11** (**Ib**), as representative examples. Significant spectral changes were observed with the addition of Cu^{2+} and Hg^{2+} while no spectral interaction was detected with Na^+, Ca^{2+}, Zn^{2+}, Cd^{2+}, Pb^{2+}, Al^{3+} and Cr^{3+} metal ions. Only, in the presence of Ni^{2+} and Co^{2+}, a quenching of about 5-10% was observed.

The most significant spectral variations in the absorption and the emission were observed in compound **24** by addition of Cu^{2+} metal ion. In the absorption spectra a decrease at 403 nm followed by an increase in the absorbance at *ca.* 345 nm was observed. In the emission spectra, a pronounced quenching in emission intensity at 442 nm is verified, as depicted in Fig. 14.

The ligand **24** and the complex **3** were the only species that interact with Hg^{2+} metal ion, whereas their absorption and emission spectra are depicted in Fig. 15. In compound **24**, a decrease in the absorbance at 403 nm is observed, as well as a quenching in the emission intensity at 442 nm. Regarding complex **3**, a decrease at 465 nm and an increase at 375 nm are noticed in the absorption spectra. Similarly, a quenching in the emission intensity is detected at 490 nm.

Regarding compound **32** and its complex **11**, no spectral changes were observed upon the addition of Cu^{2+} and Hg^{2+} metal ions. This fact could be related to the presence of one more alkyloxy chain nearby to the other.

In order to postulate the stoichiometry of the metal complexes formed in solution, the stability constants for compounds **24**/Cu^{2+}, **24**/Hg^{2+} and **3**/Hg^{2+} were determined using the HypSpec program [31]. The results suggest the formation of type L_2M_2 complexes (L = $O^{R(8)}OO^{R(8)}$) with a 2:2 (ligand to metal) stoichiometry for the interaction of β,δ-triketone **24** with the metal ions Cu^{2+} and Hg^{2+} as indicated by the values of $\log\beta\ (Cu^{2+}) = 21.51 \pm 0.04$ and $\log\beta\ (Hg^{2+}) = 18.44 \pm 0.01$. Concerning the boron complex **3**, a L'_2M type interaction was postulated (L' = $BF_2(O^{R(8)}OO^{R(8)})$), with a stoichiometry of two boron complexes for one Hg^{2+} metal ion from the obtained value of $\log\beta\ (Hg^{2+}) = 11.94 \pm 0.02$.

Compound **24** is able to detect the minimal amount of 1.33 µM and 1.00 µM by absorption, and 0.26 µM and 0.23 µM by emission of Cu^{2+} and Hg^{2+} metal ions, respectively. Regarding complex **3**, the minimal amount of 0.35 µM and 0.11 µM of Hg^{2+} metal ion was determined.

In the case of the Cu^{2+}-to-ligand interaction, the 2:2 stoichiometry was confirmed by the spectroscopic characterisation of the solid copper(II) complex of **24**, specifically synthesised according to a similar procedure described for the homologous polycatenar-containing triketonate complexes [13] and characterised as a binuclear complex of the formula $[Cu_2(O^{R(8)}OO^{R(8)})_2]$ **42** (see experimental section), and for which absorption and emission spectra were measured in THF solution (Fig. 16). The copper complex shows an absorption band at 422 nm, with an extinction molar coefficient of $6.9 \times 10^4\ M^{-1}Lcm^{-1}$. As expected, a total absence of emission was observed.

Unfortunately, the complex was not soluble in acetonitrile, chloroform or dichloromethane, preventing further studies.

4. Conclusions

Novel series of difluoroboron alkyloxyphenyl-β,δ-triketonate complexes containing peripheral substituted alkyl chains have been prepared and characterised as highly luminescent liquid crystal materials, exhibiting chemosensor ability.

The new complexes, exhibit a keto-enol tautomeric equilibrium, which was depending on the peripheral substitution. Thermal studies reveal that, in contrast to the absence of mesomorphism of the related β-diketonate complexes, all the new β,δ-triketonate derivatives behave as liquid crystal materials. The larger molecular core, the expansion of the π conjugation and the increased polarisation were proved as efficient factors to induce mesomorphism.

The smectic or columnar mesomorphism of the complexes was related to the molecular geometry, which was determined by the number and position of the peripheral flexible chains at the ligand, six-chained decorated complexes achieving the wider stability ranges of the mesophases, which even occur at room temperature.

The fluorescent emission was also found to be dependent on the substitution, showing a red shift by increasing the number of alkyl chains attached to the aromatic substituents. Likewise, the higher fluorescence efficiency was observed for compounds having restricted mobility in the excited state. Chemosensor ability of ligands and complexes towards Cu^{2+} and Hg^{2+} metal ions has been established.

In summary, modulation of the luminescent and liquid crystal properties of new boron complexes can be achieved by controlling the molecular peripheral substitution, so giving rise to polyfunctional soft materials which might offer new opportunities of research in technological fields.

Acknowledgements

We thank Dr. Rosa Claramunt and Pilar Cornago, of National University of Distance Education (Spain) for their collaboration on the solid state NMR experiments. We are grateful to the

Ministerio de Economía y Competitividad (Spain), project CTQ2011-25172. I. S. thanks the Ministerio de Educación (Spain) for the predoctoral scholarship from the FPU program. E. Oliveira acknowledges the post-doctoral grant from Fundação para a Ciência e a Tecnologia (Portugal) SFRH/BPD/72557/2010. A. F. Lodeiro thanks Fundação para a Ciência e a Tecnologia (Portugal) for the PhD grant number SFRH/BD/52528/2014. C. L. thanks to LAQV/REQUIMTE (UID/QUI/50006/2013), UCIBIO/REQUIMTE (UID/Multi/04378/2013) and PROTEOMASS Scientific Society (Portugal) for funding.

Electronic Supplementary Information

Electronic Supplementary Information (ESI) available: Full characterisation of the boron compounds, the corresponding triketones, and Figs. S1-S4 showing the full NMR assignation.

References

[1] Hepp A, Ulrich G, Schmechel R, von Seggern H, Ziessel R. Highly efficient energy transfer to a novel organic dye in OLED devices. Synth Met 2004; 146: 11-5.

[2] Benstead M, Mehl GH, Boyle RW. 4,4’-Difluoro-4-bora-3a,4a-diaza-*s*-indacenes (BODIPYs) as components of novel light active materials. Tetrahedron 2011; 67: 3573-601.

[3] Loudet A, Burgess K. BODIPY dyes and their derivatives: syntheses and spectroscopic properties. Chem Rev 2007; 107: 4891-932.

[4] Zhou Y, Xiao Y, Chi S, Qian X. Isomeric boron−fluorine complexes with donor−acceptor architecture: strong solid/liquid fluorescence and large Stokes shift. Org Lett 2008; 10: 633-6.

[5] (a) Brown NMD, Bladon P. Spectroscopy and structure of (1,3-diketonato)boron difluorides and related compounds. J Chem Soc A 1969; 526-32.

(b) Karasev VE, Korotkikh OA. Luminescence properties of boron β-diketonates. Russ J Inorg Chem 1985; 30: 1290-2.

(c) Karasev VE, Korotkikh OA. The spectral luminescent properties of BF_2 β-diketonates. Russ J Inorg Chem 1986; 31: 493-6.

(d) Chow YL, Cheng X, Johansson CI. Molecular interactions of dibenzoylmethanatoboron difluoride ($DBMBF_2$) in the excited and ground states in solution. J Photochem Photobiol A 1991; 57: 247-55.

(e) Chow YL, Johansson CI, Zhang Y-H, Gautron R, Yang L, Rassat A, Yang S-Z. Spectroscopic and electrochemical properties of 1,3-diketonatoboron derivatives. J Phys Org Chem 1996; 9: 7-16.

(f) Domercq B, Grasso C, Maldonado JL, Halik M, Barlow S, Marder SR, Kippelen B. Electron-transport properties and use in organic light-emitting diodes of a bis(dioxaborine)fluorene derivative. J Phys Chem B 2004; 108: 8647-51.

(h) Cogné-Laage E, Allemand JF, Ruel O, Baudin JB, Croquette V, Blanchard-Desce M, Jullien L. Diaroyl(methanato)boron difluoride compounds as medium-sensitive two-photon fluorescent probes. Chem-Eur J 2004; 10: 1445-55.

(i) Ono K, Yoshikawa K, Tsuji Y, Yamaguchi H, Uozumi R, Tomura M, Saito K. Synthesis and photoluminescence properties of BF_2 complexes with 1,3-diketone ligands. Tetrahedron 2007; 63: 9354-8.

(j) Nagai A, Kokado K, Nagata Y, Arita M, Chujo Y. Highly intense fluorescent diarylboron diketonate. J Org Chem 2008; 73: 8605-7.

(k) Wang D-J, Xu B-P, Wei XH, Zheng J. Preparation and spectroscopic properties of some new diaroylmethanatoboron difluoride derivatives. J Fluorine Chem 2012; 140: 49-53.

(l) Wang D-J, Kang Y-F, Xu B-P, Zheng J, Wei X-H. Synthesis, characterization and fluorescence properties of boron difluoride pyridyl-β-diketonate derivatives. Spectrochim Acta Mol Biomol Spectros 2013; 104: 419-22.

[6] Mayoral MJ, Ovejero P, Cano M, Orellana G. Alkoxy-substituted difluoroboron benzoylmethanes for photonics applications: A photophysical and spectroscopic study. Dalton Trans 2011; 40: 377-83.

[7] Sánchez I, Mayoral MJ, Ovejero P, Campo JA, Heras JV, Cano M, Lodeiro C. Luminescent liquid crystal materials based on unsymmetrical boron difluoride β-diketonate adducts. New J Chem 2010; 34: 2937-42.

[8] Sánchez I, Campo JA, Heras JV, Cano M, Oliveira E. Liquid crystal behavior induced in highly luminescent unsymmetrical borondifluoride β-diketonate materials. Inorg Chim Acta 2012; 381: 124-36.

[9] Sánchez I, Núñez C, Campo JA, Torres MR, Cano M, Lodeiro C. Polycatenar unsymmetrical β-diketonate ligands as a useful tool to induce columnar mesomorphism on highly luminescent boron difluoride complexes. J Mater Chem C 2014; 2: 9653-65.

[10] Yelamaggad CV, Achalkumar AS. Tris(N-salicylideneanilines) [TSANs] exhibiting a room temperature columnar mesophase: synthesis and characterization.Tetrahedron Lett 2006; 47: 7071-5.

[11] (a) Laschat S, Baro A, Steinke N, Giesselmann F, Hägele C, Scalia G, Judele R, Kapatsina E, Sauer S, Schreivogel A, Tosoni M. Discotic liquid crystals: from tailor-made synthesis to plastic electronics. Angew Chem Int Ed 2007; 46: 4832-87.

(b) Schmidt-Mende L, Fechtenkotter A, Mullen K, Moons E, Friend RH, MacKenzie JD. Self-organized discotic liquid crystals for high-efficiency organic photovoltaics. Science 2001; 293: 1119-22.

(c) Kumar S. Self-organization of disc-like molecules: chemical aspects. Chem Soc Rev 2006; 35: 83-109.

(d) Schmidt R, Oh JH, Sun YS, Deppisch M, Krause AM, Radacki K, Braunschweig H, Könemann M, Erk P, Bao Z, Würthner F. High-performance air-stable n-channel organic thin film transistors based on halogenated perylene bisimide semiconductors. J Am Chem Soc 2009; 131: 6215-28.

(e) Li LF, Kang SW, Harden J, Sun QJ, Zhou XL, Dai LM, Jakli A, Kumar S, Li Q. Nature-inspired light-harvesting liquid crystalline porphyrins for organic photovoltaics. Liq Cryst 2008; 35: 233-9.

(f) Xiao SX, Myers M, Miao Q, Sanaur S, Pang KL, Steigerwald ML, Nuckolls C. Molecular wires from contorted aromatic compounds. Angew Chem Int Ed 2005; 44: 7390-4.

(g) Hassheider T, Benning SA, Kitzerow HS, Achard MF, Bock H. Color-tuned electroluminescence from columnar liquid crystalline alkyl arenecarboxylates. Angew Chem Int Ed 2001; 40: 2060-3.

(h) Wendorgg JH, Christ T, Glüsen B, Greiner A, Kettner A, Sander R, Stümpflen V, Tsukruk VV. Columnar discotics for light emitting diodes. Adv Mater 1997; 9: 48-52.

[12] Dambal HK, Yelamaggad CV. Technologically promising, room temperature luminescent columnar liquid crystals derived from *s*-triazine core: molecular design, synthesis and characterization. Tetrahedron Lett 2012; 53: 186-90.

[13] Serrette AG, Lai CK, Swager TM. Complementary shapes in columnar liquid crystals: structural control in homo- and heteronuclear bimetallic assemblies. Chem Mater 1994; 6: 2252-68.

[14] (a) Lai CK, Serrette AG, Swager TM. Discotic bimetallomesogens: building blocks for the formation of new columnar arrangements of transition metals. J Am Chem Soc 1992; 114: 7948-9.

(b) Lai CK, Lin F-J. Discotic bimetallomesogens: highly disordered mesophases of columnar hexagonal arrangements in bis(tetraketonate) vanadyl and copper complexes. J Chem Soc Dalton Trans 1997; 17-20.

(c) Lai CK, Chen F-G, Ku Y-J, Tsai C-H, Lin R. Formation of disordered hexagonal arrangements in bis(β,δ-triketonato)copper(II) complexes. J Chem Soc Dalton Trans 1997; 4683-8.

(d) Lin R, Tsai C-H, Chao M-Q, Lai CK. Columnar metallomesogens: vanadyl complexes derived from β,δ-triketones. J Mater Chem 2001; 11: 359-63.

[15] Mayoral MJ, Ovejero P, Campo JA, Heras JV, Oliveira E, Pedras B, Lodeiro C, Cano M. Exploring photophysical properties of new boron and palladium(II) complexes with β-diketone pyridine type ligands: from liquid crystals to metal fluorescence probes. J Mater Chem 2011; 21: 1255-63.

[16] (a) Frigoli M, Mehl G-H. Modulation of the absorption, fluorescence, and liquid-crystal properties of functionalised diarylethene derivatives. Chem-Eur J 2004; 10: 5243-50.

(b) Dhir A, Bhalla V, Kumar M. Ratiometry of monomer/excimer emissions of dipyrenyl thiacalix[4]arene for Cu^{2+} detection: a potential Cu^{2+} and K^+ switched INHIBIT logic gate with NOT and YES logic functions. Tetrahedron Lett 2008; 49: 4227-30.

[17] (a) Liu J, Lu Y. A DNAzyme catalytic beacon sensor for paramagnetic Cu^{2+} ions in aqueous solution with high sensitivity and selectivity. J Am Chem Soc 2007; 129: 9838-9.

(b) Elanchezhian VS, Kandaswamy M. A ferrocene-based multi-signaling sensor molecule functions as a molecular switch. Inorg Chem Commun 2009; 12: 161-5.

[18] Chou S-Y, Chen C-J, Tsai S-L, Sheu H-S, Lee G-H, Lai CK. Columnar metallomesogens derived from unsymmetrical pyrazoles. Tetrahedron 2009; 65: 1130-9.

[19] (a) Berlman IB. Handbook of Fluorescence Spectra of Aromatic Molecules. 2nd ed. New York: Academic Press; 1971.

(b) Montalti M, Credi A, Prodi L, Gandolfi MT. Handbook of photochemistry. 3rd ed. Boca Raton: Taylor & Francis; 2006.

[20] Strzelecka H, Jallabert C, Veber M, Malthete J. Synthese efficace de composes aromatiques polyalcoxyles. Mol Cryst Liq Cryst 1988; 156: 347-53.

[21] Sheldrick GM. SHELX97, Program for Refinement of Crystal Structure. Göttingen, Germany: University of Göttingen; 1997.

[22] (a) Zheglova DK, Kavrakova IK, Koltsov AI, Ustynyuk YA. Mutual influence of two intramolecular hydrogen bonds in 1,3,5-triketones. J Mol Struct 1989; 195: 343-9.

(b) Novak P, Skare D, Sekusak S, Vikic-Topic D. Substituent, temperature and solvent effects on keto-enol equilibrium in symmetrical pentane-1,3,5-triones. Nuclear magnetic resonance and theoretical studies. Croat Chem Acta 2000; 73: 1153-70.

[23] Kuo H-M, Cheng H-W, Sheu H-S, Lai CK. Room temperature mesogens formed by H-bonded Schiff-bases α,β,γ-triketonates. Tetrahedron 2013; 69: 5945-54.

[24] Nakamoto K. Infrared and Raman Spectra of Inorganic and Coordination Compounds. 6th ed. Hoboken, New Jersey: John Wiley & Sons; 2009.

[25] Dierking I. Textures of Liquid Crystals. Germany: Wiley-VCH; 2003.

[26] Cuerva C, Campo JA, Ovejero P, Torres MR, Cano M. Polycatenar pyrazole and pyrazolate ligands as building blocks of new columnar Pd(II) metallomesogens. Dalton Trans 2014; 43: 8849-60.

[27] (a) Abe Y, Akao H, Yoshida Y, Takashima H, Tanase T, Mukai H, Ohta K. Syntheses, structures, and mesomorphism of a series of Ni(II) salen complexes with 4-substituted long alkoxy chains. Inorg Chim Acta 2006; 359: 3147-55.

(b) Abe Y, Takagi Y, Nakamura M, Takeuchi T, Tanase T, Yokokawa M, Mukai H, Megumi T, Hachisuga A, Ohta K. Structural, photophysical, and mesomorphic properties of luminescent platinum(II)-salen Schiff base complexes. Inorg Chim Acta 2012; 392: 254-60.

(c) Sun E-J, Sun Z-Y, Yuan M, Wang D, Shi TS. The synthesis and properties of meso-tetra(4-alkylamidophenyl)porphyrin liquid crystals and their Zn complexes. Dyes Pigments 2009; 81: 124-30.

[28] Gallardo H, Ferreira M, Vieira AA, Westphal E, Molin F, Eccher J, Bechtold IH. Columnar mesomorphism of bent-rod mesogens containing 1,2,4-oxadiazole rings. Tetrahedron 2011; 67: 9491-9.

[29] (a) Lin YC, Lai CK, Chang YC, Liu KT. Formation of hexagonal columnar phases by heterocyclic pyrimidine derivatives. Liq Cryst 2002; 29: 237-42.

(b) Lai CK, Tsai CH, Pang YS. Discotic metallomesogens: mesophase crossover of columnar rectangular to hexagonal arrangements in bis(hydrazinato)nickel(II) complexes. J Mater Chem 1998; 8: 1355-60.

[30] (a) Lavallee RJ, Palmer BJ, Billing R, Hennig H, Ferraudi G, Kutal C. Efficient substitutional photochemistry of a third-row transition metal β-diketonate domplex. Inorg Chem 1997; 36: 5552-8.

(b) Lewis FD, Salvi GD, Kanis DR, Ratner MA. Electronic structure and spectroscopy of nickel(II), palladium(II), and platinum(II) acetylacetonate complexes. Inorg Chem 1993; 32: 1251-8.

[31] Gans P, Sabatini A, Vacca A. Investigation of equilibria in solution. Determination of equilibrium constants with the HYPERQUAD suite of programs. Talanta 1996; 43: 1739-53.

Table 1

$[BF_2(HO^{R(n)}OO^{R(n)})]$	n	no.	n	no.	$[BF_2(HO^{R(n)2}OO^{R(n)2})]$	n	no.
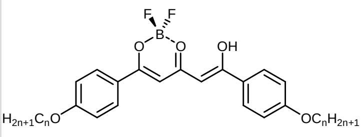 **Ia**	4	**1**	12	**5**	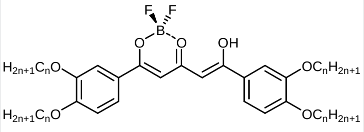 **Ib**	12	**9**
	6	**2**	14	**6**		14	**10**
	8	**3**	16	**7**		16	**11**
	10	**4**	18	**8**		18	**12**
$[BF_2(HO^{R'(n)2}OO^{R'(n)2})]$	n	no.			$[BF_2(HO^{R(n)3}OO^{R(n)3})]$	n	no.
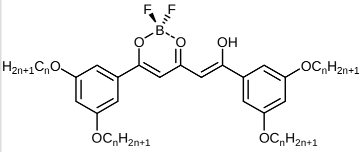 **Ic**	12	**13**			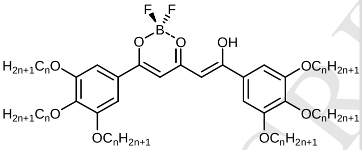 **Id**	12	**17**
	14	**14**				14	**18**
	16	**15**				16	**19**
	18	**16**				18	**20**
$[HO^{R(n)}OO^{R(n)}H]$	n	no.	n	no.	$[HO^{R(n)2}OO^{R(n)2}H]$	n	no.
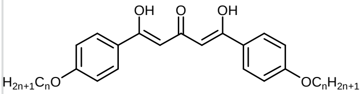 **IIa**	1	**21**			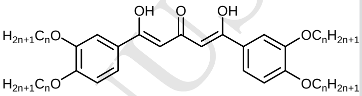 **IIb**	12	**30**[a]
	4	**22**	12	**26**[a]		14	**31**[a]
	6	**23**[a]	14	**27**[a]		16	**32**[a,b]
	8	**24**[a]	16	**28**[a]		18	**33**
	10	**25**[a]	18	**29**			
$[HO^{R'(n)2}OO^{R'(n)2}H]$	n	no.			$[HO^{R(n)3}OO^{R(n)3}H]$	n	no.
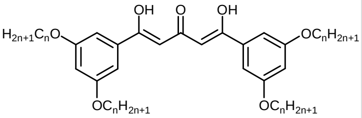 **IIc**	12	**34**			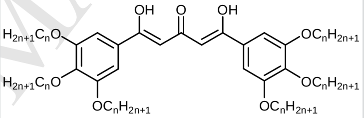 **IId**	12	**38**[b]
	14	**35**				14	**39**[b]
	16	**36**				16	**40**[b]
	18	**37**				18	**41**

[a] Previusly reported in ref. [18]. [b] Previusly reported in ref. [13].

Table 2

Empirical formula	$C_{19}H_{18}O_5$
Formula weight	326.33
Crystal system	Orthorhombic
Space group	$P2_12_12_1$
Space group number	19
a / Å	5.7567(5)
b / Å	8.6513(7)
c / Å	33.125(3)
V / Å^3	1649.7(2)
Z	4
T / K	293(2)
F(000)	688
ρ_c / g cm^{-3}	1.314
μ / mm^{-1}	0.095
Scan technique	ω and φ
Data collected	(-6, -10, -39) to (6, 10, 33)
θ range (º)	1.23 to 25.00
Reflections collected	12543
Independent reflections	2901 (R_{int} = 0.0470)
Completeness to maximum θ (%)	99.9
Data / restraints / parameters	2901 / 0 / 218
Observed reflections [$I > 2\sigma(I)$]	1596
R^a	0.0457
$R_{wF}{}^b$	0.1496

^{a} $\Sigma[|F_o| - |F_c|] / \Sigma[|F_o|$. ^{b} $\{\Sigma[w(F_o{}^2 - F_c{}^2)^2] / \Sigma[w(F_o{}^2)^2]\}^{1/2}$

Table 3.

Compound	**24** (**IIa**)	**30** (**IIb**)	**34** (**IIc**)	**38** (**IId**)
−COCH_2CO	4.26	4.25	4.26	4.26
−CC*H*CO	5.91	5.90	5.95	5.91
	6.93	6.23	6.23	6.22
−CO*H*	14.87	14.91	14.72	14.85
	16.08	16.08	15.84	16.24

[a] Measured in $CDCl_3$ (δ in ppm)

Table 4. Characteristic signals on ^{13}C-NMR spectra of compound **24** (**IIa**)^{a}

	CDCl$_3$ solution			Solid state	
Nucleus	**II$_1$**	**II$_2$**	**II$_3$**	**II$_2$**	**II$_3$**
C-1	193.7	189.9	173.7	192.8	173.1
C-2	50.8	96.4	96.4	97.6	95.0
C-3	192.8	173.7	189.8	167.8	193.8
C-4	95.8	96.4	96.4	94.9	95.3
C-5	183.0	164.1	173.7	162.7	173.1

$^{a}\delta$ in ppm

Table 5.

C1 – C2	1.367(5)	C1 – C2 – C3	123.5(4)
C2 – C3	1.419(5)	C3 – C4 – C5	123.2(3)
C3 – C4	1.432(5)	O1 – C1 – C2	120.5(4)
C4 – C5	1.351(4)	C2 – C3 – O2	120.3(4)
C1 – O1	1.331(4)	O2 – C3 – C4	119.5(3)
C3 – O2	1.281(4)	C4 – C5 – O3	120.0(5)
C5 – O3	1.337(4)		

Table 6.

D – H ··· A	d(D – H)	d(H ··· A)	d(D ··· A)	<(D – H·· A)
O3 – H3 ··· O2	1.23	1.44	2.515(4)	140.3
O1 – H1 ··· O2	1.01	1.69	2.551(4)	140.4

Table 7.

		Enol	Keto
^{1}H-NMR	–CO*H*	11.40	
	–CC*H*(2)CO	6.25	6.64
	–CC*H*(4)COH	5.92	4.15
^{19}F-NMR	BF_2	–143	–139
^{13}C-NMR	C-1	192.5	193.2
	C-2	92.6	94.4
	C-3	173.7	179.9
	C-4	97.2	52.3
	C-5	190.7	208.9

$^{a}\delta$ in ppm

Table 8.

	Compound	*n*	Transition^{a}	T /ºC^{b}	ΔH/kJmol^{-1}		Compound	*n*	Transition^{a}	T /ºC^{b}	ΔH/kJmol^{-1}
IIa	**22**	4	Cr → Cr’	96		**IIb**	**30**	12	Cr → Cr’	79	11.4
			Cr’ → I	100	48.9^{d}				Cr’ → Cr’’	92	2.8
	23	6	Cr → Cr’	97					Cr’’ → I	111	44.7
			Cr’ → I	100	38.7^{d}		**31**	14	Cr → Cr’	82	
	24	8	Cr → Cr’	82	11.4				Cr’ → Cr’’	87	22.2^{d}
			Cr’ → I	103	35.2				Cr’’ → I	108	68.2
	25	10	Cr → Cr’	86			**32**	16	Cr → Cr’	53	
			Cr’ → I	99	40.2^{d}				Cr’ → Cr’’	67	57.6^{d}
	26	12	Cr → Cr’	67	0.9				Cr’’ → I	82	1.2
			Cr’ → I	105	48.1		**33**	18	Cr → Cr’	61	
	27	14	Cr → Cr’	72	27.3				Cr’ → Cr’’	65	
			Cr’ → I	107	56.6				Cr’’ → I	72^{c}	11.7^{d}
	28	16	Cr → Cr’	76	13.1	**IIc**	**34**	12	Cr → I	59	114.6
			Cr’ → I	104	67.3		**35**	14	Cr → I	58	90.5
	29	18	Cr → Cr’	83	8.4		**36**	16	Cr → I	57	81.7
			Cr’ → I	102	73.7		**37**	18	Cr → I	58	97.8
						IId	**38**	12	Cr → I	53	78.3
							39	14	Cr → I	67	87.6
							40	16	Cr → Cr’	50	77.2
									Cr’ → I	71	67.1
							41	18	Cr → Cr’	57	53.7
									Cr’ → I	77	80.1

[a]Cr, Cr’ = crystalline phases, I = isotropic liquid. [b]DSC peak temperatures. [c]Detected by POM. [d]Overlapped processes.

Table 9.

	Compound	*n*	Transition^a	T /ºC^b	ΔH/kJmol^{-1}		Compound	*n*	Transition^a	T /ºC^b	ΔH/kJmol^{-1}
Ia	**1**	4	Cr → I	134	32.6		**10**	14	Cr → SmA	47^c	
			I → Cr	107	−12.4				SmA → Cr’	59	−18.3
	2	6	Cr → Cr’	102	1.4				Cr’ → I	84	35.0
			Cr’ → I	117	14.4		**11**	16	Cr → Cr’	57	
			I → Cr	108	−10.3				Cr’ → SmA	63^c	103.7^d
	3	8	Cr → Cr’	88	8.9				SmA → Cr’’	72^c	−68.2
			Cr’ → I	128	23.5				Cr’’ → I	82	19.9
			I → Cr	119	−22.1		**12**	18	Cr → Cr’	58c	
			Cr’ → Cr	78	−1.0				Cr’ → SmA	65	144.0^d
	4	10	Cr → I	127	30.5				SmA → Cr’’	75	−82.3
			I → Cr	119	−24.7				Cr’’ → I	88	50.1
	5	12	Cr → Cr’	88	13.2	**Ic**	**13**	12	Cr → Col$_L$	51	51.8
			Cr’ → I	128	31.5				Col$_L$ → I	61	0.8
			I → Cr	120	−27.2		**14**	14	Cr → Col$_L$	55^c	
			Cr’ → Cr	84	−5.6				Col$_L$ → I	62	55.9^d
	6	14	Cr → I	132	49.0		**15**	16	Cr → Col$_L$	58^c	
			I → Cr	126	−45.5				Col$_L$ → I	71	99.6^d
	7	16	Cr → Cr’	103	41.0		**16**	18	Cr → Col$_L$	60^c	
			Cr’ → SmC	114					Col$_L$ → I	77	141.6^d
			SmC → I	120	35.4^d	**Id**	**17**	12	Col$_h$ → I	68^c	
			I → SmC → Cr	108^d	−35.5^d				I → Col$_h$	62^c	
			Cr’ → Cr	87	−23.0		**18**	14	Cr → Col$_h$	43^c	
	8	18	Cr → Cr’	105					Col$_h$ → I	71	34.3^d
			Cr’ → SmC	114					I → Col$_h$	61^c	
			SmC → I	122	78.4^d		**19**	16	Cr → Col$_h$	48	44.3
			I → SmC → Cr	116^d	−48.0^d				Col$_h$ → I	66	49.5
			Cr’ → Cr	91	−15.5				I → Col$_h$	53^c	
Ib	**9**	12	Cr → SmA	27^c					Col$_h$ → Cr	44	−49.7
			SmA → Cr’	54	−87.8		**20**	18	Cr → Col$_h$	57	42.0
			Cr’ → I	78	43.3				Col$_h$ → I	81	65.0
									I → Col$_h$	65	−58.4
									Col$_h$ → Cr	49	−15.4

^{a}Cr, Cr’ = crystalline phases, SmC = smectic C mesophase, SmA = smectic A mesophase, Col$_L$ = discotic lamellar mesophase, Col$_h$ = hexagonal columnar mesophase, I = isotropic liquid. ^{b}DSC peak temperatures. ^{c}Detected by POM. ^{d}Overlapped processes.

Table 10.

Compound	Phase	2θ (º)	$d_{\text{obs}}{}^{a}$ (Å)	$d_{\text{calc}}{}^{a}$ (Å)	$[hkl]^{b}$	Parameters^{c}
7	SmC	2.2	39.6	39.6	001	T = 115 ºC^{d}
(**Ia**)		2.4	20.1	19.8	002	d = 39.9 Å
		19.5	4.5	-	-	
12	SmA	1.6	56.4	56.4	001	T = 68 ºC^{d}
(**Ib**)		3.2	27.8	28.2	002	d = 57.0 Å
		4.7	18.9	18.8	003	
		5.9	14.9	14.1	004	
		19.5	4.5	-	-	
15	Col_{L}	3.5	25.5	25.5	001	T = 60 ºC^{d}
(**Ic**)		7.0	12.7	12.7	002	d = 25.5 Å
		19.5	4.5	-	-	
16	Col_{L}	3.3	26.5	26.5	001	T = 64 ºC^{d}
(**Ic**)		6.5	13.6	13.3	002	d = 27.1 Å
		9.6	9.2	8.9	003	
		19.5	4.5	-	-	
19	Col_{h}	3.0	29.6	29.6	100	T = 60 ºC^{d}
(**Id**)		5.2	17.1	17.1	110	a = 34.3 Å
		5.9	15.0	14.8	200	
		7.9	11.2	11.2	210	
		22.1	4.0	-	001	
		19.5	4.5	-		
20	Col_{h}	2.7	32.4	32.4	100	T = 65 ºC^{d}
(**Id**)		4.7	19.7	18.7	110	a = 36.6 Å
		5.4	16.3	16.2	200	
		7.9	11.2	12.2	210	
		22.2	4.0	-	001	
		19.5	4.5	-	-	

$^{a}d_{\text{obs}}$ and d_{calc} are the measured and calculated diffraction spacings. $^{b}[hkl]$ are the Miller indices of the reflections. ^{c}For lamellar phases: lamellar periodicity $d = (\sum l d_{00l})/\text{N}_{00l}$, where N_{00l} is the number of $00l$ reflections. For hexagonal columnar phases: lattice constant $a = \sum d_{hk}\sqrt{(h^{2} + k^{2} + hk)}/\sqrt{(3\text{N}_{hk})}$, where N_{hk} is the number of $hk0$ reflections.[9,26,28] ^{d}On heating

Table 11.

Comp.	Type	Number of chains	n	$\lambda_{\mathrm{abs}}^{\mathrm{max}}$ /nm ^{a}	ε / 10^4 $\mathrm{Lmol^{-1}cm^{-1}}$	$\lambda_{\mathrm{emis}}^{\mathrm{max}}$ /nm ^{a}	ϕ_{F}^{b}	$\Delta\lambda$ /nm ^{c}	$\lambda_{\mathrm{em(solid)}}^{\mathrm{max}}$/nm ^{a}
3	**Ia**	2	8	281	3.5	490	0.36	25	593
				372	2.6				
				440sh	3.9				
				465	4.6				
5	**Ia**	2	12	286	2.1	490	0.34	25	590
				374	1.8				
				442sh	2.8				
				465	3.5				
10	**Ib**	4	14	330	0.7	483	0.67	50	560
				384	1.7				
				433	1.3				
11	**Ib**	4	16	330	0.9	483	0.71	50	560
				384	2.3				
				433	1.3				
15	**Ic**	4	16	286	1.2	496	0.04	31	543
				372	1.0				
				443sh	1.6				
				465	1.9				
19	**Id**	6	16	286	6.7	534	0.11	67	600
				376	2.8				
				474	2.6				
20	**Id**	6	18	284	5.2	525	0.11	90	581
				377	1.8				
				435	1.0				
24	**IIa**	2	8	330	1.8	442	0.02	39	520
				403	2.9				
26	**IIa**	2	12	330	1.6	442	0.02	39	495
				403	2.0				
31	**IIb**	4	14	270	1.4	455	0.005	108	500
				299	1.0				
				347	7.6				
				400	5.8				
32	**IIb**	4	16	270	1.4	418	0.003	83	487
				300	1.5				
				335	1.7				
				398	2.1				
36	**IIc**	4	16	330	2.3	450	0.008	59	490
				391	1.5				
40	**IId**	6	16	330	2.4	470	0.04	61	511
				409	1.2				
41	**IId**	6	18	330	2.1	469	0.05	60	520
				409	0.6				

[a] Estimated error: ±1 nm (sh = shoulder). [b] Estimated error: ±5 %. [c] Stokes shift

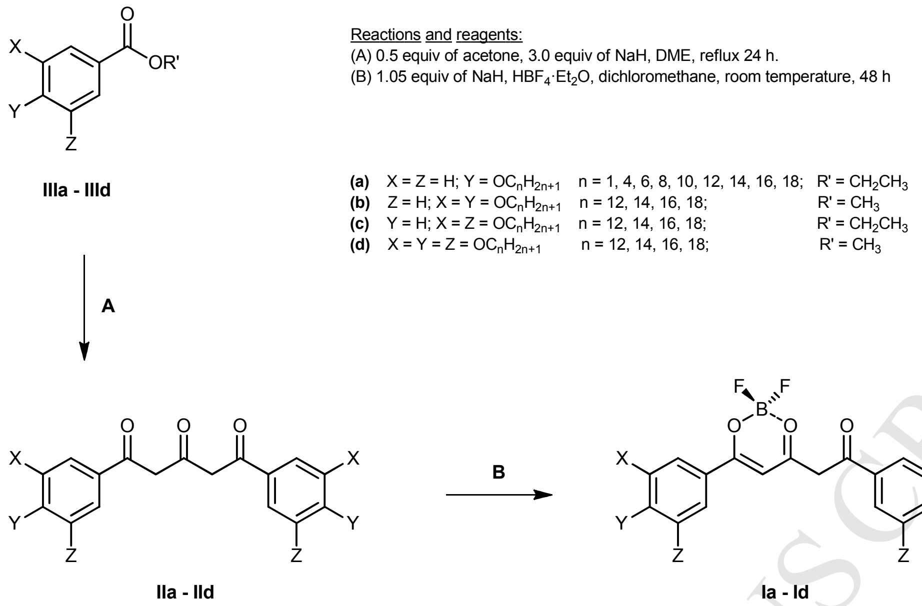

Reactions and reagents:
(A) 0.5 equiv of acetone, 3.0 equiv of NaH, DME, reflux 24 h.
(B) 1.05 equiv of NaH, $HBF_4 \cdot Et_2O$, dichloromethane, room temperature, 48 h

(a) X = Z = H; Y = OC_nH_{2n+1} n = 1, 4, 6, 8, 10, 12, 14, 16, 18; R' = CH_2CH_3
(b) Z = H; X = Y = OC_nH_{2n+1} n = 12, 14, 16, 18; R' = CH_3
(c) Y = H; X = Z = OC_nH_{2n+1} n = 12, 14, 16, 18; R' = CH_2CH_3
(d) X = Y = Z = OC_nH_{2n+1} n = 12, 14, 16, 18; R' = CH_3

Scheme 1

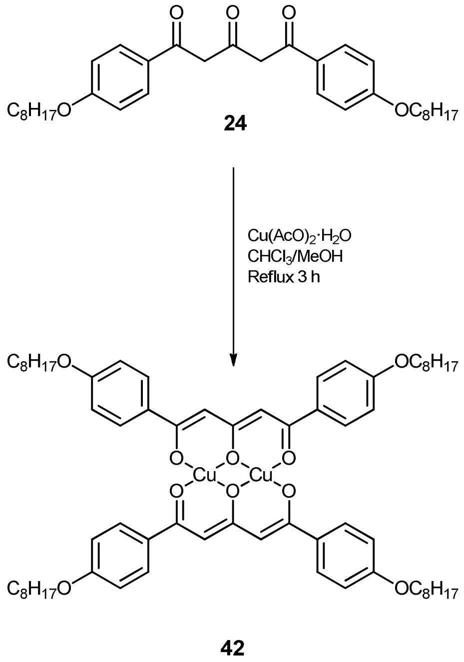
O
O
O
$C_8H_{17}O$
OC_8H_{17}
24
$Cu(AcO)_2·H_2O$
$CHCl_3$/MeOH
Reflux 3 h
$C_8H_{17}O$
OC_8H_{17}
O
Cu
O
Cu
O
O
O
O
$C_8H_{17}O$
OC_8H_{17}
42

Scheme 2

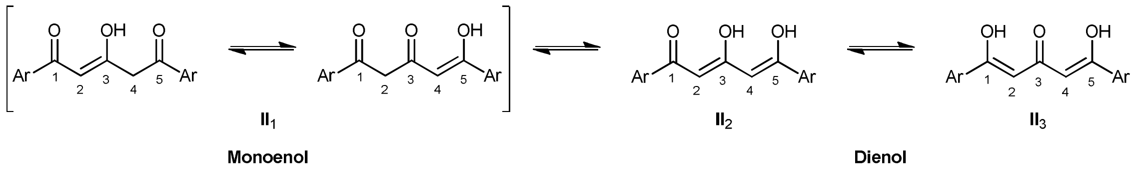

Ar = C_6H_5-*p*-OC_8H_{17}

Figure 1

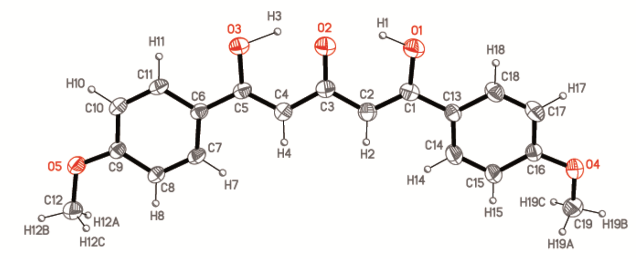
H3
O2
H1
O1
O3
H11
H18
C11
C18
H10
C6
C4
C2
C13
H17
C10
C5
C3
C1
C17
C7
C14
H4
H2
O5
C9
C16
O4
C8
H7
H14
C15
C12
H19C
H8
H15
H12A
C19
H19B
H12B
H12C
H19A

Figure 2

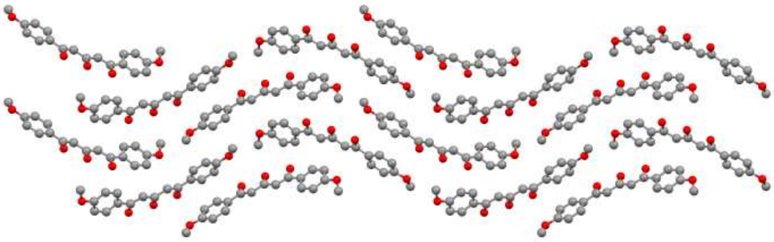

Figure 3

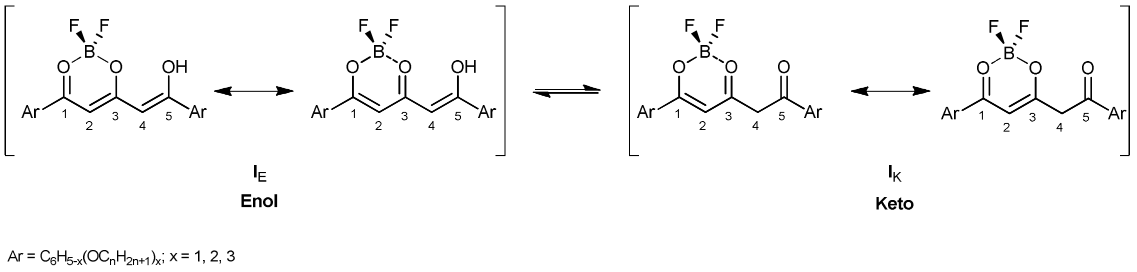
F
F
B
O
O
OH
Ar
Ar
1
2
3
4
5
O
$\mathbf{I}_E$
Enol
$\mathbf{I}_K$
Keto
Ar = $C_6H_{5-x}(OC_nH_{2n+1})_x$; x = 1, 2, 3

Figure 4

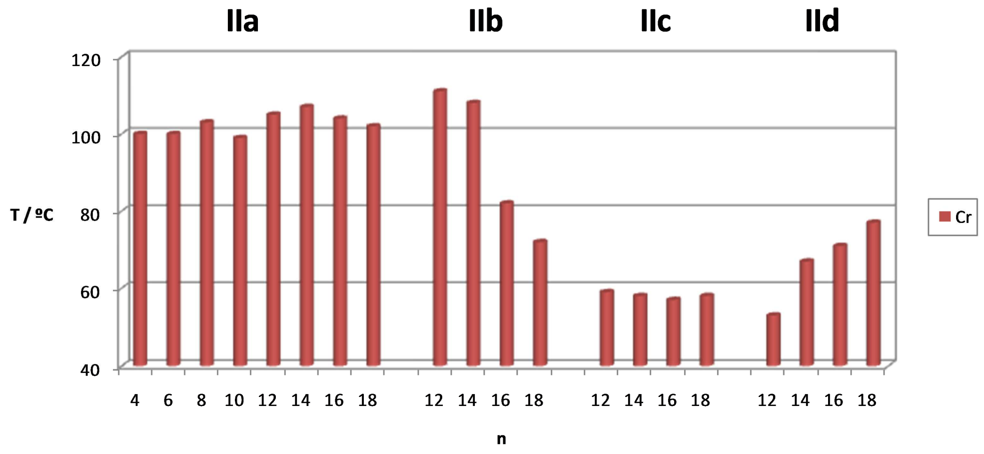
IIa
IIb
IIc
IId
120
100
80
60
40
T / ºC
Cr
4
6
8
10
12
14
16
18
12
14
16
18
12
14
16
18
12
14
16
18
n

Figure 5

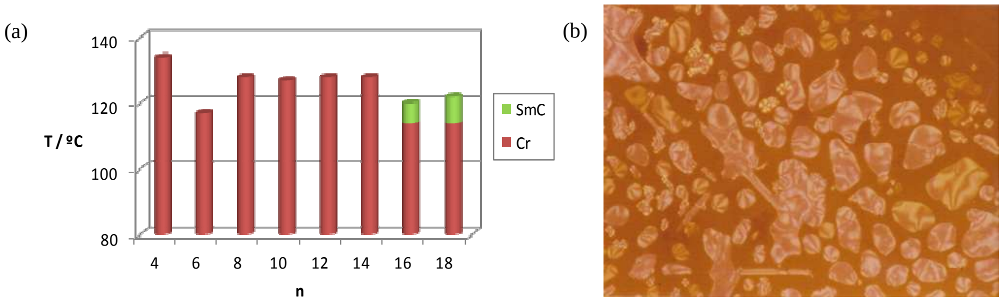

Figure 6

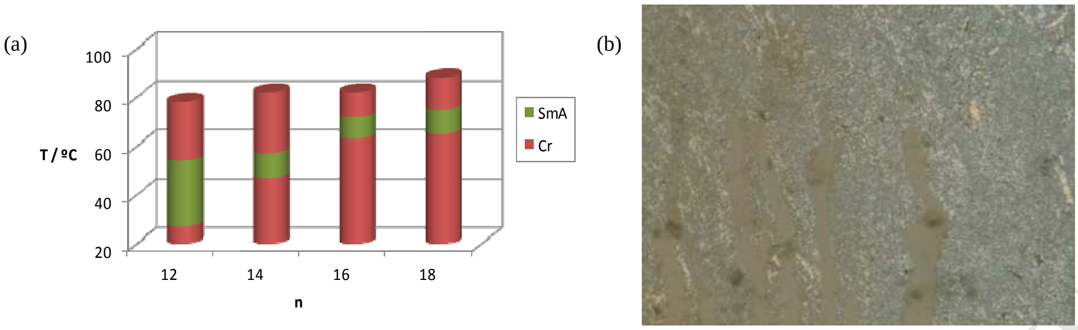

Figure 7

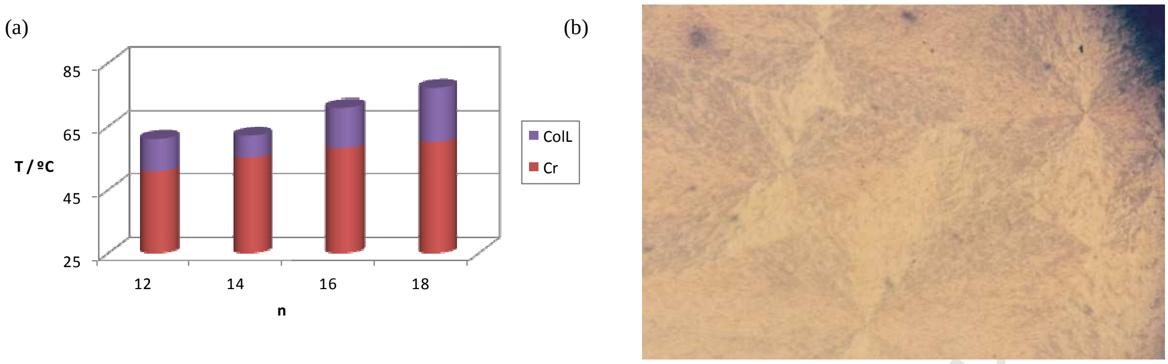

Figure 8

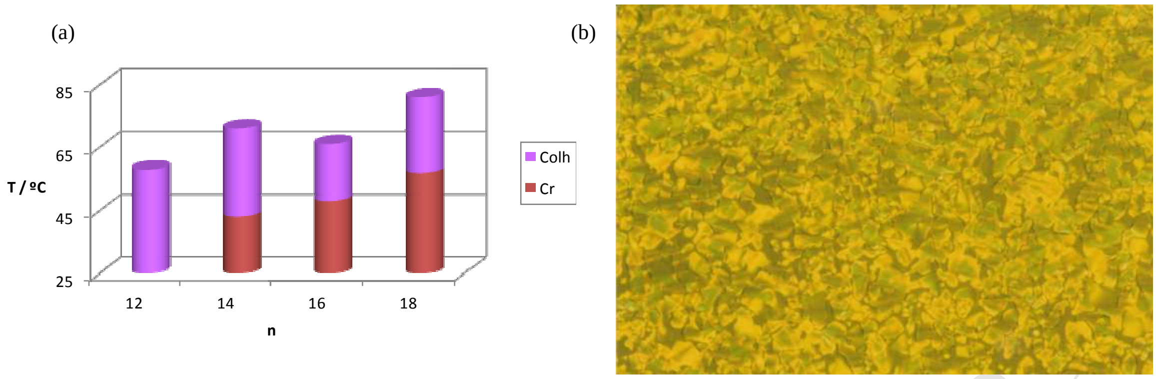

Figure 9

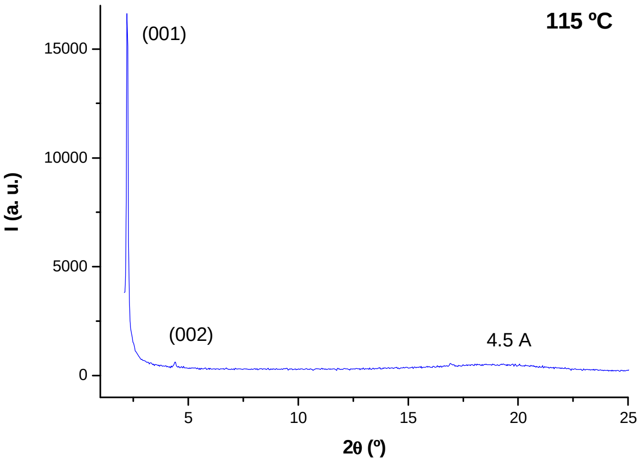

Figure 10

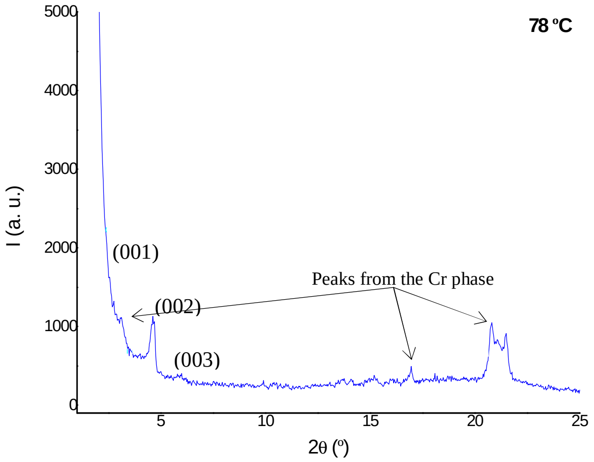
78 ºC
5000
4000
3000
2000
1000
0
I (a. u.)
(001)
(002)
(003)
Peaks from the Cr phase
5
10
15
20
25
2θ (º)

Figure 11

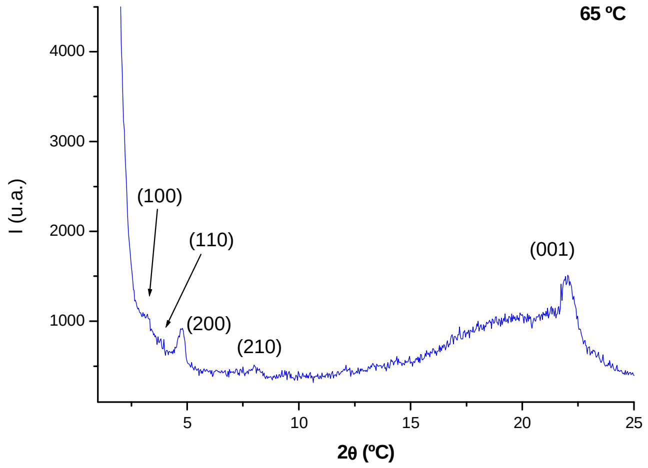
65 ºC
I (u.a.)
4000
3000
2000
1000
(100)
(110)
(200)
(210)
(001)
5
10
15
20
25
2θ (ºC)

Figure 12

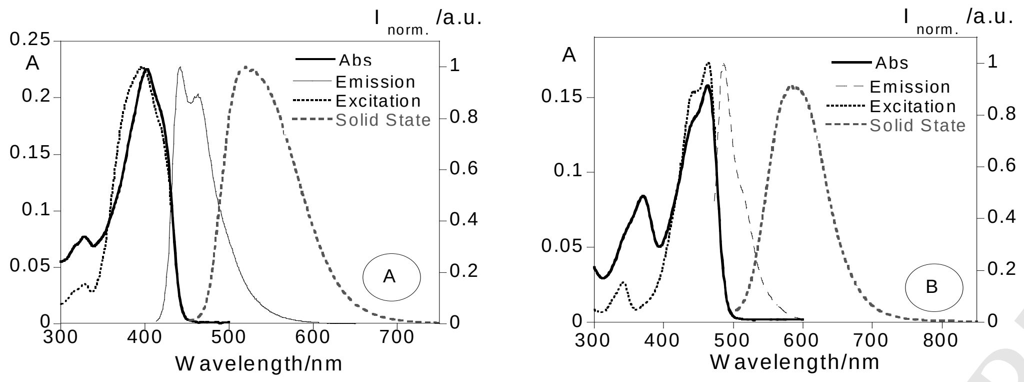
A
0.25
0.2
0.15
0.1
0.05
0
300
400
500
600
700
Wavelength/nm
I norm. /a.u.
1
0.8
0.6
0.4
0.2
0
Abs
Emission
Excitation
Solid State
A
A
0.15
0.1
0.05
0
300
400
500
600
700
800
Wavelength/nm
I norm. /a.u.
1
0.8
0.6
0.4
0.2
0
Abs
Emission
Excitation
Solid State
B

Figure 13

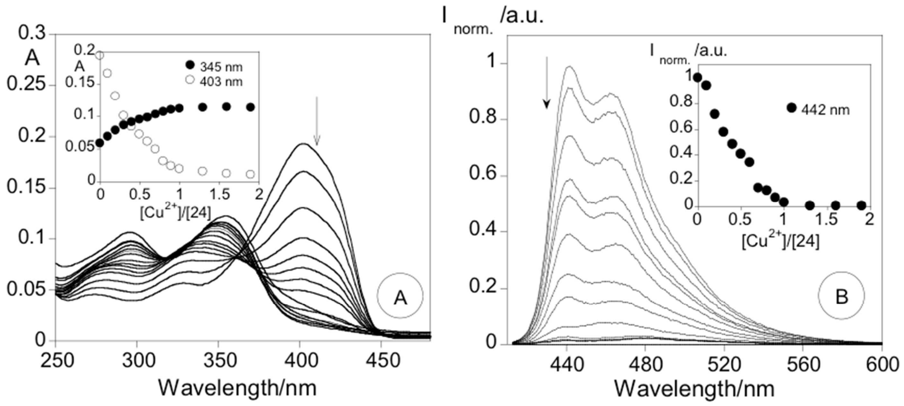
A
0.3
0.25
0.2
0.15
0.1
0.05
0
250
300
350
400
450
Wavelength/nm
A
0.2
0.15
0.1
0.05
0
0
0.5
1
1.5
2
[Cu2+]/[24]
● 345 nm
○ 403 nm
A
I norm. /a.u.
1
0.8
0.6
0.4
0.2
0
440
480
520
560
600
Wavelength/nm
I norm. /a.u.
1
0.8
0.6
0.4
0.2
0
0
0.5
1
1.5
2
[Cu2+]/[24]
● 442 nm
B

Figure 14

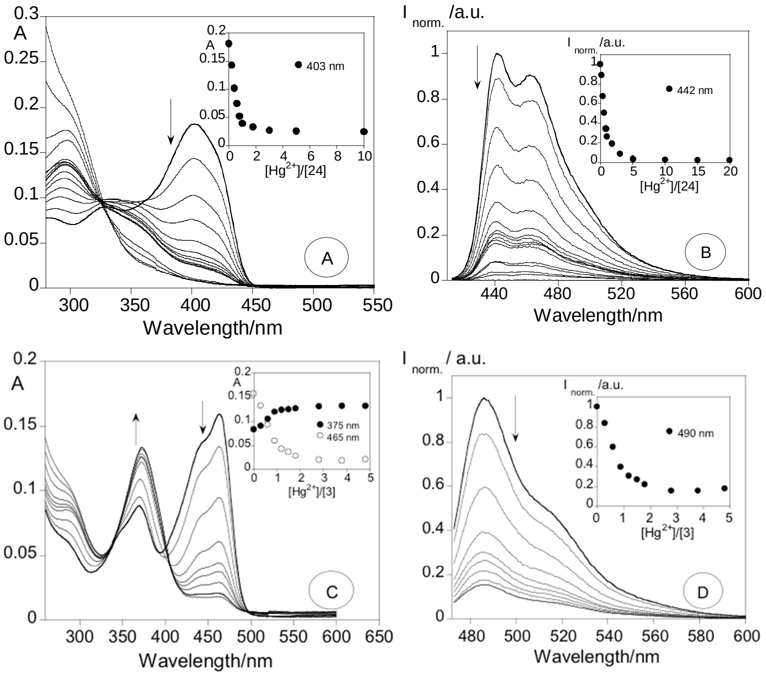
A
0.3
0.25
0.2
0.15
0.1
0.05
0
300 350 400 450 500 550
Wavelength/nm
403 nm
[Hg2+]/[24]
A
I norm. /a.u.
442 nm
440 480 520 560 600
Wavelength/nm
B
A
375 nm
465 nm
[Hg2+]/[3]
300 350 400 450 500 550 600 650
Wavelength/nm
C
I norm. / a.u.
490 nm
480 500 520 540 560 580 600
Wavelength/nm
D

Figure 15

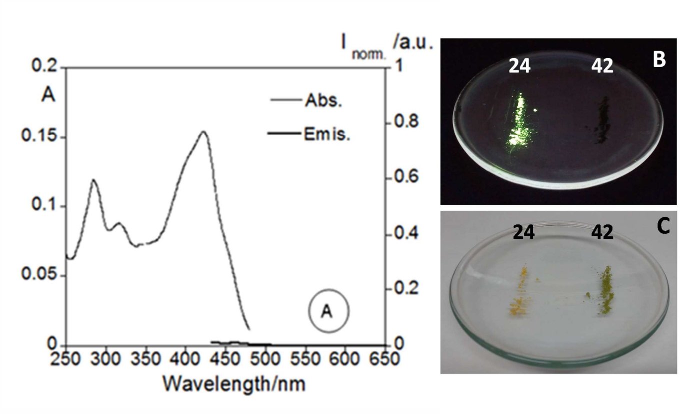
A
0.2
0.15
0.1
0.05
0
250 300 350 400 450 500 550 600 650
Wavelength/nm
I norm. /a.u.
1
0.8
0.6
0.4
0.2
0
Abs.
Emis.
A
B
24
42
C
24
42

Figure 16

CAPTIONS FOR TABLES

Table 1. Numbering and nomenclature of the compounds I and II studied in this work

Table 2. Crystal and refinement data for **21**

Table 3. Characteristic signals^{a} on ^{1}H-NMR spectra for selected derivatives [HO$^{R(n)x}$HOO$^{R(n)x}$] **II**

Table 4. Characteristic signals on ^{13}C-NMR spectra of compound **24** (**IIa**)^{a}

Table 5. Selected bond distances (Å) and angles (º) for **21**

Table 6. Hydrogen bond geometries (distances in Å and angles in degrees)

Table 7. Characteristic NMR signals for **3** (**Ia**)^{a}

Table 8. Phase behaviour of compounds **22-41** (**II**) determined by DSC and POM

Table 9. Phase behaviour of compounds **1-20** (**I**) determined by DSC and POM

Table 10. X-Ray diffraction data

Table 11. Photophysical data of **3**, **5**, **15**, **19**, **20**, **24**, **26**, **36**, **40**, **41** in dichloromethane solution and in solid state at 295 K

LEGENDS FOR FIGURES AND SCHEMES

Scheme 1. Synthetic route of ligands **II** and complexes **I**

Scheme 2. Synthesis of [Cu_2(O$^{R(8)}$OO$^{R(8)}$)$_2$] **42**

Figure 1. Keto-enol tautomeric equilibrium observed by solution NMR studies on compounds **II**

Figure 2. ORTEP plot of [HO$^{R(1)}$OO$^{R(1)}$H] **21** with 20 % probability

Figure 3. Packing of **21** where corrugated layers are established

Figure 4. Keto-enol equilibrium established by NMR studies for derivatives **Ia** and **Ic**

Figure 5. Bar diagram representing the melting temperatures for compounds **II**

Figure 6. (a) Bar diagram representing the phases ranges of compounds **Ia**. (b) Microphotograph of **7** at 115 ºC on cooling showing a *Schlieren* texture

Figure 7. (a) Bar diagram representing the phases ranges of compounds **Ib**. (b) Microphotograph of **12** at 70 ºC on heating showing a texture with oily strikes

Figure 8. (a) Bar diagram representing the phases ranges of compounds **Ic**. (b) Microphotograph of **15** at 60 ºC on cooling showing a broken fan-like texture

Figure 9. (a) Bar diagram representing the phases ranges of compounds **Id**. (b) Microphotograph of **18** at 54 ºC on cooling showing a mosaic texture

Figure 10. X-Ray diffraction pattern of **7** (**Ia**) at 115 ºC on heating

Figure 11. X-Ray diffraction pattern of **12** (**Ib**) at 78 ºC on heating

Figure 12. X-Ray diffraction pattern of **20** (**Id**) at 65 ºC on heating

Figure 13. Absorption (bold line), excitation (dotted line) and emission spectra (full line) in CH_2Cl_2 solution and in the solid state (grey line) at room temperature of compound **24** (A) and complex **3** (B) (λ_{exc24} = 403 nm; λ_{exc3} = 465 nm). [**24**] = 6.7 x 10^{-6} M, [**3**] = 4.4 x 10^{-6} M, T = 295 K)

Figure 14. Spectrophotometric (A) and spectrofluorimetric (B) titrations of compound **24** in dichloromethane solution as a function of increasing amounts of Cu^{2+} metal ion in acetonitrile. The inset (A) represent the absorption read at 345 nm and 403 nm, and the inset (B) the emission at 442 nm. (λ_{exc24} = 403 nm, [**24**] = 4.4 x 10^{-6} M, T = 295 K)

Figure 15. Spectrophotometric (A, C) and spectrofluorimetric (B, D) titrations of compound **24** (A, B) and complex **3** (C, D) in CH_2Cl_2 with the addition of Hg^{2+} metal ion. The insets represent the absorption (A, C) and the emission intensity (B, D) as a function of [Hg^{2+}]/[**24**], [Hg^{2+}]/[**3**] at 403 nm for (A), 375 nm and 465 nm for (C), 442 nm for (B) and 490 nm for (D), respectively. (λ_{exc24} = 403 nm; λ_{exc3} = 465 nm). [**24**] = 6.7 x 10^{-6} M, [**3**] = 4.4 x 10^{-6} M, T = 295 K)

Figure 16. (A) – Absorption and emission spectra of the copper complex **42** in THF. ([**42**] = 2.88 × 10^{-6} M, λ_{exc} = 422 nm). Naked eye (C) and under UV lamp (B) (λ = 365 nm) images of compound **24** and its copper complex **42**

Triketonate difluoroboron complexes. Substitution-dependent liquid crystal and photophysical properties

Ignacio Sánchez,[a] Adrián Fernández-Lodeiro,[b,c] Elisabete Oliveira,[b,c] José Antonio Campo,[a] M. Rosario Torres,[d] Mercedes Cano,*[a] and Carlos Lodeiro*[b,c]

New alkoxyphenyl-substituted β,δ-triketonate difluoroboron complexes have been prepared

The mesomorphic behaviour was depending on the substitution of the triketonate ligand

Fluorescence was also proved to be dependent on the ligand substitution

The fluorescence was maintained in the mesophase

These multifunctional materials also present luminescent sensor activity